NASA MEMO 3-5-59A

NASA

MEMORANDUM

STABILITY AND CONTROL CHARACTERISTICS AT SUBSONIC SPEEDS OF A FLAT-TOP ARROWHEAD WING-BODY COMBINATION

By Donald A. Buell and Norman S. Johnson

Ames Research Center
Moffett Field, Calif.

Declassified March 12, 1963

NATIONAL AERONAUTICS AND SPACE ADMINISTRATION

WASHINGTON

March 1959

NATIONAL AERONAUTICS AND SPACE ADMINISTRATION

MEMORANDUM 3-5-59A

STABILITY AND CONTROL CHARACTERISTICS AT SUBSONIC SPEEDS OF A FLAT-TOP ARROWHEAD WING-BODY COMBINATION

By Donald A. Buell and Norman S. Johnson

SUMMARY

A wind-tunnel investigation was made to determine the longitudinal- and lateral-stability derivatives of a flat-top wing-body configuration at Mach numbers from 0.22 to 0.90 and Reynolds numbers of 3.5 and 17 million. The wing had a leading-edge sweepback of 78.9° and a cathedral of 45° on the outer panels. The tests included the determination of the effectiveness of elevon and rudder controls and also an investigation of ground effects. The model was tested at angles of attack up to 28° and angles of sideslip up to 18°.

The dynamic response of this configuration has been determined from the wind-tunnel data for a simulated airplane having a wing loading of 17.7 pounds per square foot. The longitudinal data show a forward shift in aerodynamic center of 10 percent of the mean aerodynamic chord as the lift coefficient is increased above 0.1. Although flown in the lift range of decreasing stability, the simulated airplane did not encounter pitch-up in maneuvers initiated from steady level flight with zero static margin unless a load factor of 2.2 was exceeded. This maneuver margin was provided by a large value of pitching moment due to pitching velocity. The number of cycles to damp the Dutch roll mode to half amplitude, the time constants of the roll subsidence and spiral divergence modes, and control effectiveness in roll are computed. The lateral stability is shown to be positive but is marginal in meeting the military specifications for today's aircraft.

An analog computer study has been made in five degrees of freedom (constant velocity) which illustrates that the handling characteristics are satisfactory. Several programed rolling maneuvers and coordinated turns also illustrate the handling qualities of the airplane.

INTRODUCTION

Tests reported in references 1 and 2 have demonstrated the potentialities of a configuration having a flat-top arrowhead wing for achieving efficient flight at high supersonic speeds. However, the practicality of such a configuration may depend upon the ease with which it is brought to rest at its destination. It was, therefore, desired to establish the stability and control characteristics of the configuration at subsonic speeds and, particularly, at landing speeds. To this end, a model similar to one of reference 2 was tested in the Ames 12-foot pressure wind tunnel. The results were used in an analog computer study to simulate a representative airplane flying at low speeds. The computer study was particularly useful since the dynamics of such an unusual configuration are not readily interpreted from wind-tunnel data. The investigation included the determination of the control effectiveness of "wing-tip elevons" and of a rudder mounted on a ventral fin. Ground effects on the static stability characteristics were also measured.

NOTATION

In this report the lift and drag data are referred to the usual wind axes. All other forces and moments are referred to body axes. The longitudinal axis of this reference system passes through the moment center and is parallel to the lower surface of the wing. The coefficients are defined as follows:

C_D drag coefficient, $\frac{\text{drag}}{(\rho/2)V^2S}$

C_l rolling-moment coefficient, $\frac{\text{rolling moment}}{(\rho/2)V^2Sb}$

C_L lift coefficient, $\frac{\text{lift}}{(\rho/2)V^2S}$

C_m pitching-moment coefficient, $\frac{\text{pitching moment}}{(\rho/2)V^2S\bar{c}}$

C_n yawing-moment coefficient, $\frac{\text{yawing moment}}{(\rho/2)V^2Sb}$

C_Y side-force coefficient, $\frac{\text{side force}}{(\rho/2)V^2S}$

P_b base-pressure coefficient, $\frac{p_b - p_\infty}{(\rho/2)V^2}$

$C_{m_{\dot{\alpha}}}, C_{m_q}$ derivatives with respect to subscript times $\frac{\bar{c}}{2V}$

$C_{l_{\dot{\beta}}}, C_{n_{\dot{\beta}}}, C_{l_p}, C_{n_p}, C_{l_r}, C_{n_r}$ derivatives with respect to subscript times $\frac{b}{2V}$

M_α $\frac{\partial}{\partial \alpha}\left(\frac{\text{pitching moment}}{I_{YY}}\right)$

M_q $\frac{\partial}{\partial q}\left(\frac{\text{pitching moment}}{I_{YY}}\right)$

Z_α $\frac{\partial}{\partial \alpha}\left(\frac{\text{-lift}}{m}\right)$

The dynamic derivatives were measured and are presented in combinations which represent the total moment about the appropriate axis when the model was oscillated about the moment center. Other symbols used are defined as follows:

b developed wing span

$\bar{c}$ wing mean aerodynamic chord

$C_{1/2}$ cycles to damp to one-half amplitude

g acceleration due to gravity

h height of moment center above ground plate

I_{XX}, I_{YY}, I_{ZZ} moments of inertia about the X,Y, and Z body axes

I_{XZ} product of inertia about X and Z axes

M Mach number

m mass

n_Z	ratio of normal force to weight
p	rolling velocity
p_b	static pressure at base
p_∞	static pressure in free stream
q	pitching velocity
r	yawing velocity
R	Reynolds number based on $\bar{c}$
S	wing area of developed plan form, including area over fuselage ahead of juncture between wing trailing edge and fuselage
t	time
v_e	$V\beta\sqrt{\rho/\rho_o}$, ft/sec
V	free-stream velocity
x	distance from nose of model parallel to longitudinal axis
$\frac{\Delta x}{\bar{c}}$	center-of-gravity shift in forward direction, in chord lengths
α	angle of attack of longitudinal axis
β	angle of sideslip
δ_a	aileron deflection, difference between elevon deflections; positive to increase rolling moment
δ_e	elevon deflection, positive to increase elevon lift (indicates one-half of total elevon deflection if subscript "left" or "right" is not added)
δ_r	rudder deflection, positive to increase side force
$\Delta(\ )$	increment of ( )
ζ	ratio of damping to critical damping
ρ	free-stream density
ρ_o	density of air at sea level

τ	time constant, time to accomplish approximately 63 percent of commanded change
φ	angle of roll
$\frac{\lvert\varphi\rvert}{\lvert v_e \rvert}$	ratio of roll angle in degrees to equivalent sideslip velocity
ω_n	natural frequency
$(\dot{})$	derivative with respect to time

MODEL AND APPARATUS

Figure 1(a) is a drawing of the model and figure 1(b) shows the model mounted in the wind tunnel over a ground plate (to be described). The wing of the model was an aluminum plate, flat on the lower surface and increasing in thickness away from the leading edge with a blunt trailing edge. The thickness to chord ratio was about 0.02. The wing had a leading-edge sweepback of 78.9°, a cathedral of 45° on the outer panels, an area of 3.448 square feet, and an aspect ratio of 1.03. The wing surface corresponding to these dimensions includes all of the fuselage area which lies forward of the wing trailing-edge and fuselage intersection.

The elevons (control surfaces at the wing tips) were attached with flush brackets bent to the desired angle. The rudder was the rear part of the ventral fin, and deflections were obtained by bending the soft steel fins to the desired angles. The fuselage consisted of sheet aluminum in the form of a half-body of revolution with its axis inclined 1° to the wing lower surface.

Static forces and moments on the model were measured on a six-component strain-gage balance inside the fuselage. The balance was supported by a sting which had a diameter of 2.9 inches just aft of the fuselage but which increased to 4 inches aft of the wing trailing edge. Another sting used less extensively had a constant diameter of 2 inches.

The dynamic derivatives of the model were evaluated by means of an oscillation apparatus similar to that described in reference 3. For such measurements the model was mounted on crossed flexure pivots enclosed by the fuselage. In this particular investigation the flexure pivots were so oriented that the model rotation consisted of pure pitching, yawing, or rolling about body axes. The oscillations were excited and maintained by a push rod passing down the center of the sting to an electromagnetic shaker downstream of the model. The shaker was controlled by an electronic feedback network which maintained a preset oscillation amplitude at the natural frequency of the model and support system. The deflection and

aerodynamic moments were measured by means of strain gages and processed through an analog computing system in order to evaluate the derivatives. The sting for the oscillation tests had a diameter of 2-1/4 inches aft of the fuselage and a diameter of 3 inches aft of the wing trailing edge.

The presence of the ground was simulated by a plate which spanned the wind tunnel. This plate is the one described in reference 4. The model was situated in the wind tunnel such that the moment center was about 68 inches behind the leading edge of the plate. A slot exists in the rear of the plate to accommodate the sting at high angles of attack. For the present investigation the slot was sealed back to a point aft of the trailing edge of the model at low or moderate angles of attack and to a point even with the elevon hinge line at the highest angles of attack.

TESTS

Static-force tests of the model were made with the 4-inch-diameter sting and no ground plate. The longitudinal characteristics of the model were determined for angles of attack up to 22°. In order to determine the lateral and directional characteristics, the sideslip angle was varied up to 18° at angles of attack of 3-1/2°, 6-3/4°, 9-3/4°, and 12-1/2°. In addition, lateral-force measurements were made at sideslip angles of 0° and 6° with varying angle of attack. To evaluate control effectiveness the elevons were deflected to angles as great as ±20° and the rudder to angles as great as 30° in both variable sideslip and variable angle-of-attack tests. Other static-force tests were made to determine the longitudinal and lateral characteristics with the 2-inch-diameter sting at angles of attack up to 14°. The longitudinal characteristics and the elevon effectiveness of the model on the 4-inch sting were also measured in the presence of the ground plate at angles of attack to 28°. The ventral fin was taken off the model for the ground-plate tests to allow the model to be brought near the plate.

The dynamic derivatives of the model were evaluated at an average sideslip angle of 0° through an angle-of-attack range up to 16°. The angle of oscillation was approximately ±1.6° for all measurements except damping in pitch, where only half this amplitude could be achieved at some angles of attack. Other measurements at smaller amplitudes showed little effect of amplitude. The reduced frequency of the oscillation ($\omega\bar{c}/2V$ or $\omega b/2V$) varied from 0.18 to 0.04. In these parameters only V, the free-stream velocity of the test, varied to any extent.

All configurations of the model were tested at a Mach number of 0.22, and selected configurations were also tested at 0.80 and 0.90. All tests except one were made at a Reynolds number of about 3.5 million based on the mean aerodynamic chord. The exception was a test to measure static longitudinal characteristics at a Reynolds number of 17.5 million.

CORRECTIONS TO DATA

The data were corrected for the constriction effects of the tunnel walls by the method of reference 5. This correction amounted to slightly more than 1/2 percent of the Mach number and dynamic pressure at the highest test Mach number.

Calculations of the induced effects of the tunnel walls made by the method of reference 6 indicated that such corrections were small enough to be ignored. In these calculations the trailing edges of the plan form were assumed to be straight. The maximum indicated error from this source was 0.2° in the angle of attack, 0.002 in drag coefficient, and 0.001 in pitching-moment coefficient. The induced effects of the tunnel walls with the ground plate installed were calculated by the method outlined in reference 4. For this case the corrections were even smaller than those quoted above and were also ignored.

No corrections were applied to the data for sting interference. It was presumed that the vehicle represented by the model would normally glide without power in the subsonic speed range. Therefore, the base pressures which would be experienced by the vehicle were considered to be more closely approximated by the actual base pressure on the model than by the free-stream static pressure to which drag data are sometimes adjusted. However, the base pressures were measured and are presented.

Simulation of the ground by a plate is imperfect because of the presence of a boundary layer on the plate. The pressure measurements showed little difference between the boundary layer for this investigation and that for the tests in reference 4. The displacement thickness was about 1/8 inch at the station of the moment center of the model. It was concluded that the flow angle induced by the plate was of the same order of magnitude as that caused by tunnel walls and was negligible.

Moment tares representing the nonaerodynamic damping of the oscillation mechanism were subtracted from the dynamic data. These tares were determined by oscillating the model with no free-stream velocity at various static pressures and extrapolating to a pressure of zero. The tares were typically less than 10 percent of the aerodynamic moments except in the case of the roll derivatives. The tares due to rolling were equivalent to values of C_{l_p} and C_{n_p} of about 0.01.

AIRPLANE SIMULATION

Geometric and mass characteristics for the representative airplane which were used to determine the dynamic characteristics from the wind-tunnel data are given below:

S	1,075 sq ft
W	19,000 lb
$\bar{c}$	40 ft
I_{XX}	24,900 slug-ft^2
I_{YY}	192,000 slug-ft^2
I_{ZZ}	216,900 slug-ft^2
I_{XZ}	-1,600 slug-ft^2
b	32.5 ft

Vertical c.g. location is 0.76 ft below wing lower surface.

From the wind-tunnel data it was determined that the following equations approximate the moment and lift curves for the center of gravity located at $0.55\bar{c}$:

$$C_m = 0.0127 - 0.0552\delta_e + 0.379(\alpha - 0.1334\delta_e)^2 , \quad \delta_e < 5^\circ \qquad (1)$$

$$C_m = 0.00795 - 0.0818(\delta_e - 0.0873) + 0.379[\alpha - 0.0116 - 0.220(\delta_e - 0.0873)]^2 , \quad \delta_e > 5^\circ \qquad (2)$$

$$C_L = -0.020 + 0.1146\delta_e + 1.173\alpha , \quad 0^\circ < \alpha < 4^\circ \qquad (3)$$

$$C_L = 0.062 + 0.1146\delta_e + 1.722(\alpha - 0.070) , \quad 4^\circ < \alpha < 8^\circ \qquad (4)$$

$$C_L = 0.182 + 0.1146\delta_e + 2.235(\alpha - 0.140) , \quad 8^\circ < \alpha \qquad (5)$$

For the above equations, positive elevon deflection is down; computations show that δ_e is larger than 5° for all trim angles of attack considered. The angles α and δ_e are measured in radians to evaluate C_m and C_L as indicated above. The term "elevator deflection" is used to indicate deflection of the elevons so as to provide a pitching moment and no rolling moment.

The lateral coefficients were taken to be linear functions of sideslip angle within $\pm 4^\circ$ of sideslip. The term "aileron deflection" is used to indicate deflection of the elevons so as to produce a rolling moment.

The following equations were used to simulate the airplane in five degrees of freedom. The equations are written as though the derivatives are linear; however, the appropriate variation of the derivative and control effectiveness with angle of attack or sideslip as indicated by the wind-tunnel data was incorporated into the simulation:

$$\dot{\alpha} = q - \beta p - C_L \frac{(\rho/2)SV}{m} + \frac{g}{V} \cos \varphi \tag{6}$$

$$\dot{q} = C_m \frac{(\rho/2)V^2 S\bar{c}}{I_{YY}} + C_{m_q} q \frac{(\rho/4)SV\bar{c}^2}{I_{YY}} - rp \left(\frac{I_{XX}-I_{ZZ}}{I_{YY}}\right) - (p^2-r^2) \frac{I_{XZ}}{I_{YY}} \tag{7}$$

$$\dot{\beta} = \alpha p - r + [C_{Y_\beta}\beta + C_Y(\delta_a,\delta_r)] \frac{(\rho/2)SV}{m} + \frac{g}{V} \sin \varphi \tag{8}$$

$$\dot{p} = (\dot{r}+pq) \frac{I_{XZ}}{I_{XX}} - qr \frac{I_{ZZ}-I_{YY}}{I_{XX}} + (C_{l_p}p+C_{l_r}r) \frac{(\rho/4)SVb^2}{I_{XX}} + [C_{l_\beta}\beta+C_l(\delta_a,\delta_r)] \frac{(\rho/2)SV^2 b}{I_{XX}} \tag{9}$$

$$\dot{r} = (\dot{p}-qr) \frac{I_{XZ}}{I_{ZZ}} - pq \left(\frac{I_{YY}-I_{XX}}{I_{ZZ}}\right) + (C_{n_r}r+C_{n_p}p) \frac{(\rho/4)SVb^2}{I_{ZZ}} + [C_{n_\beta}\beta+C_n(\delta_r,\delta_a)] \frac{(\rho/2)SV^2 b}{I_{ZZ}} \tag{10}$$

The damping derivative $C_{m_q} + C_{m_{\dot{\alpha}}}$ as measured in the wind tunnel was assumed equal to C_{m_q} in the simulation, and $C_{m_{\dot{\alpha}}}$ was assumed zero. Derivatives with respect to $\dot{\beta}$ were similarly neglected. All calculations were made for sea-level density.

RESULTS AND DISCUSSION

Longitudinal Characteristics

The static longitudinal characteristics of the model with all control surfaces neutral are presented in figure 2. The pitching-moment data for low speeds show large losses in stability with increasing lift. Forward shifts in the aerodynamic center were as much as $0.1\bar{c}$ as the lift coefficient increased from 0.1. Below this lift coefficient the stability was

about neutral. Data from reference 2 show that forward positions of the center of gravity would be detrimental to the trim drag at hypersonic speeds. Consequently, the maximum lift coefficient obtainable at low speeds with a positive static margin is quite limited when the center of gravity is located to achieve high lift-drag ratios at hypersonic speeds.

The drag due to lift shown in figure 2 varies from $C_L \tan \alpha$ by an amount which is within the experimental scatter. This characteristic shows that there was little leading-edge suction and indicates the presence of flow separation at the leading edge. The increase in the lift curve slope near 4° angle of attack is thought to identify the start of the leading-edge separation and the establishment of a leading-edge "vortex" such as is discussed in reference 7. On this model, unlike a delta wing, the center of lift moved forward after the leading-edge separation commenced. An example of the linear stability characteristics of a low-aspect-ratio delta wing is given in reference 8. This reference also presents results of low-speed tests on configurations similar to the present model and shows the effects of various plan-form modifications.

A fivefold increase in Reynolds number was slightly adverse to the low-lift static stability, while an increase in Mach number to 0.90 greatly improved the high-lift stability. Data taken with the smaller sting, although not shown, almost duplicated the data of figure 2. The chief differences caused by the reduction in sting diameter were an increase in zero-lift drag of 0.001 to 0.002, and an increase in lift at the higher Mach numbers of about 3 percent.

The longitudinal characteristics of the model near the ground are shown in figure 3. An improvement in stability resulted from decreasing the ground height, but it should be pointed out that the lowest ground height is an extreme, inasmuch as the ventral fin would strike the ground at a very small angle of attack.

The longitudinal characteristics of the model with various deflections of the elevons are presented in figure 4. Most of the data pertain to the model with only the left elevon deflected. However, the pitching moments due to 10° deflection of both elevons are just twice those due to 10° deflection of one elevon within the experimental accuracy. The only noticeable nonlinearity in the variation of pitching moment with elevon deflection occurred at negative deflections and angles of attack less than 12°. Except for this range, the elevon effectiveness increased with angle of attack. Figure 5 presents the increments of pitching-moment coefficient due to elevon deflection and shows that there was no effect of Mach number on elevon effectiveness.

Figure 5 also shows typical values of the pressure coefficient at the base of the model. If free-stream static pressure were to be the base pressure instead of that shown in the figure, the drag coefficients

of the model would be decreased by 0.007 to 0.013. In tests with the 2-inch-diameter sting the base-pressure coefficients were slightly more negative. The maximum differences were 15 to 20 percent at angles of attack near 10°.

The effects of sideslip angle on the pitching moments are shown in figure 6. A mild loss of static longitudinal stability due to sideslip is indicated by the fact that C_m increases more with angle of attack at the higher sideslip angles than at 0°. The effect is more pronounced at the higher Mach numbers.

Figure 7 presents pitch-damping data for the model and shows that the damping was positive under all test conditions. At the higher Mach numbers data were obtained only at elevon deflections which brought the static moments on the model approximately into balance. This kept the model deflections within the physical limits of the model support system. Little effect of elevon deflection was apparent where comparative data were available.

The foregoing data have been applied to the calculation of several stability parameters for the representative airplane. With a certain amount of data smoothing, the static margin has been computed as a function of landing speed and is given in figure 8. Neutral static stability at a landing speed of 300 feet per second and a lift coefficient of 0.165 can be achieved by shifting the center of gravity forward approximately 4 percent of $\bar{c}$. This speed and center-of-gravity location were selected as a basis for analyzing the dynamic behavior of the airplane. It is recognized that this forward shift in center of gravity would increase the trim drag at hypersonic speeds, but the increase is estimated to be less than 5 percent.

Pitch-up is of primary concern since the moment derivative M_α becomes positive as angle of attack increases. For accelerated flight an added restoring moment is supplied by the pitching moment due to pitching velocity. The simulated airplane is then stable as long as the restoring moment $-M_\alpha + (Z_\alpha/V)M_q > 0$. This criterion is plotted in figure 9 as a function of angle of attack at a velocity of 300 feet per second and a center-of-gravity location of $0.51\bar{c}$. The criterion for static stability, $-M_\alpha$, is also shown so that the effect of damping can be readily noted. Figure 9 also shows that for angles of attack larger than 6° the airplane is at least critically damped ($\zeta = 1$).

The existence of this added stability in pitch-up was verified by a simulation study in which the response of the airplane to elevator steps was recorded. The maneuver was initiated from trim angle of attack at 300 feet per second. Location of the center of gravity was found at which the

commanded normal acceleration could just be achieved without pitch-up instability. The results are plotted in figure 10. It can be seen that with zero static margin the airplane may approach a load factor of 2.2 without encountering pitch-up.

Time histories showing the longitudinal oscillatory characteristics for the airplane as simulated on the analog computer are shown in figure 11. These runs were made for a landing speed of 300 feet per second with the center of gravity at $0.51\bar{c}$, the point of zero static margin for this speed. Responses are shown for both an elevator step and pulse. Note that the elevator step maneuver is controllable up to a maneuver of $n_Z = 2$ even though the slope of the moment curve becomes positive with increasing angle of attack.

Lateral Characteristics

The effect of elevon deflection on the lateral force and moment coefficients for the model at low speeds is shown in figure 12(a). The configuration is such that elevon deflections provide substantial moments about all three axes. As in the case of pitch, the roll and yaw effectiveness of the elevons increased somewhat with angle of attack except for negative deflections at small angles of attack. In the latter case, the yawing moments departed considerably from the approximately linear variation with deflection angle that existed elsewhere.

Although an airplane similar to this model could conceivably be controlled with elevon deflections only, the possibility of directional control with less rolling moment by either a rudder or a split-flap type elevon was the basis for further model tests. The results are shown in figures 12(b) and 12(c) with a $\pm\delta_e$ identifying the angle of the split-flap surfaces above and below the neutral position. The figures show that the rudder effectiveness was approximately constant with varying angle of attack. The effectiveness of the split flap decreased at the larger deflections while that of the rudder increased. It can be seen that the rudder created a rolling moment which was approximately half as much as the elevon produced for the same yawing moments.

The effects of Mach number on the control effectiveness are shown in figure 13 in the form of incremental force or moment coefficients due to elevon deflection. An increase in Mach number decreased the effectiveness of the split-flap type elevon as a directional control (fig. 13(b)).

Tests in the presence of the ground plate included tests with one elevon deflected. Results of these tests showed there were no ground effects on elevon effectiveness.

The static lateral-directional characteristics of the model with control surfaces neutral are presented in figures 14 and 15. Figure 14 shows that the variations of the coefficients with sideslip angles from 0° to -6° are approximately linear except in the case of C_n at angles of attack above $6\text{-}1/2^\circ$. With this exception the data of figure 15 are considered to be representative of the variation of static stability with angle of attack. Figure 12 shows that there is a small rolling moment at 0° sideslip at the higher angles of attack, evidently as a result of model asymmetry. Though not shown, this rolling-moment coefficient was the same for all Mach numbers and would slightly change the apparent rolling moments due to sideslip indicated in figure 15.

The variation of C_n with β was approximately linear at sideslip angles less than $\pm 4^\circ$. Values of C_{n_β} in this small sideslip region varied by as much as 50 percent as the angle of attack was increased from 0° to $12\text{-}1/2^\circ$. The maximum values of C_{n_β} occurred near $9\text{-}1/2^\circ$. Tests were also made of the model at an angle of attack near $12\text{-}1/2^\circ$ on the 2-inch-diameter sting. These data (not shown) demonstrated that the sting had a large effect on the directional stability at sideslip angles greater than $\pm 4^\circ$. In this region, reducing the sting diameter changed C_n by as much as 0.005. The yawing-moment coefficients at large angles of attack and sideslip are therefore not considered representative of a flying vehicle. The sting diameter had no other noticeable effects on the lateral characteristics of the model.

Some static lateral characteristics with various control surface deflections are shown in figure 16. Positive deflections of the elevons had little effect on the stability, but the large negative deflections generally increased the directional stability. The most extensive stability changes were caused by a negative deflection of the elevon on the leading wing. The geometry of this configuration is such that the local angle of attack of the leading wing at its outer panel decreases with sideslip angle. A negative elevon deflection will also be likely to make the local angle of attack more negative at the outer panel. Thus, the largest change in stability due to control deflection occurs when the angle of attack is small or negative and is probably associated with the elimination of the leading-edge vortex over part of the wing. Nonlinearities in control effectiveness have also been noted, at negative elevon deflections and small angles of attack, which may be also expected to arise from changes in the leading-edge vortex on the outer wing panel.

It is assumed that the stalling of the rudder at the larger angles of sideslip is responsible for the loss of effectiveness shown in figure 16.

Figure 17 presents the lateral dynamic derivatives of the model. The damping in roll and yaw was positive at all angles of attack of the test. The least desirable characteristic at angles of attack up to 16° may well be the negative yawing moment due to rolling velocity. Large roll excitations of a representative airplane would be anticipated

because of the large dihedral effect and the small damping and inertia in roll which is inherent in wings of low aspect ratio. When combined with large roll excitations, the negative yawing moment due to roll might lead to poor damping characteristics of the short period lateral oscillation. It is to be noted that an airplane of this configuration would have a principal axis naturally inclined at a positive angle to the longitudinal axis. Such a weight distribution would tend to counteract the unfavorable moments considered above. The effect of Mach number on the dynamic derivatives was small at most angles of attack and confined mainly to the yawing-moment derivatives.

To illustrate the effects of the aerodynamic characteristics as presented in figures 14, 15, and 17 on a representative airplane, the cycles to damp the Dutch roll oscillatory mode to one-half amplitude, $C_{1/2}$, have been computed for several angles of attack. The stability, represented by the inverse of $C_{1/2}$, is shown in figure 18 versus $|\varphi|/|v_e|$. Also included is a minimum acceptable boundary as specified by the military in reference 9. The variation in stability results primarily from the increase in dihedral effect as angle of attack increases. It should be noted that C_{l_β} has been reduced from the values indicated by the wind-tunnel data by moving the center of gravity higher (from 0.06 b below the wing to 0.02 b below the wing). It can be seen that the stability characteristics improve at high angles of attack which is, in part, a result of a reduction in the large negative values of C_{n_p}. A similar plot is given in figure 19 showing the effect of velocity and center-of-gravity position on Dutch roll characteristics for trim angles of attack. Increasing the landing velocity definitely improves the stability characteristics, but there are obvious limitations to improvement due to this effect. When the curves in figures 18 and 19 are compared to the present flying-qualities specifications, it should be remembered that landing lateral-stability requirements may be modified considerably for a high-speed configuration such as this. Time histories for the Dutch roll oscillation at 300 feet per second velocity with the c.g. at $0.51\bar{c}$ are given in figure 20.

Two other factors of importance to the dynamic analysis, the inverse of the time constant for the roll subsidence and spiral divergence modes, are presented in figure 21. Increasing the effective dihedral increases the stability of the spiral mode, and this effect is also shown in figure 21. Here the spiral mode is seen generally to become more stable with angle of attack, as did the effective dihedral.

The roll-control effectiveness is presented in figure 22. When the dihedral effect and directional stability combine with the aileron control in yaw and roll such that

$$C_{n_\beta} C_{l_{\delta_a}} < C_{l_\beta} C_{n_{\delta_a}}$$

the restoring rolling moment applied by the aileron will be overcome by the rolling moment induced by the sideslip due to the aileron yawing moment. The aileron moments therefore produce static instability when

$$C_{n_\beta} - \frac{C_{l_\beta} C_{n_{\delta_a}}}{C_{l_{\delta_a}}} < 0$$

This is the quantity which is plotted in figure 22. No instability is evident.

Analog Simulation of Landing Maneuvers in Five Degrees of Freedom (Constant Velocity)

To evaluate the handling characteristics of the flat-top arrowhead-wing configuration, the following maneuvers were programed into an analog computer simulation study:

1. Rolls from -45° to +45° roll angle

2. Rolls from trim angle of attack and 0° roll angle to 45° roll angle with and without a programed longitudinal coordinated maneuver

3. A turn consisting of a roll to a given roll angle and an increase in normal acceleration to maintain level flight

Aileron rolls from -45° to +45° roll angle.- To perform this maneuver the airplane started from a 1.4g coordinated turn position and rolled 90° to a similar position turning in the opposite direction. The maneuver was commanded with a step aileron input which was held constant for the 90° change in roll angle and then returned to zero. The value of the aileron step was a parameter which was varied to evaluate the effect of roll rate. A typical time history of this maneuver is given in figure 23. As the command was returned to zero when $\varphi = 45°$, an overshoot in roll angle occurred, and the roll angle continued to change. The yawing moments which induced sideslip forces during roll are indicated by the angle of sideslip since no resisting yawing moments are applied through a rudder. Figure 24(a) shows the maximum allowable roll rate to restrict this angle of sideslip to 1° as a function of the landing approach speed. Also shown for comparison is the roll rate to obtain $pb/2V = 0.05$. Figure 24(b) shows the normal accelerations induced by this maneuver as a function of the landing speed. A velocity of 300 feet per second shows minimum longitudinal coupling.

Aileron rolls from 0° to 45° roll angle.- Aileron rolls were made from 0° to 45° roll with and without an increase in normal acceleration to develop a constant rate horizontal turn. A typical time history of this maneuver is given in figure 25. Figure 26(a), which presents induced sideslip as a function of aileron deflection, illustrates that increase of normal acceleration during roll has no effect on sideslip. Figure 26(b) gives the change in normal acceleration as a function of aileron deflection and shows that the initial normal acceleration induced by roll is unchanged by coordination of the rolling maneuver, but in this case the final value is changed. The command was an aileron step input which returned to zero after the airplane had rolled 45°. The magnitude of the aileron step was varied to evaluate the effect of roll rate.

Level flight turn.- Figure 27 shows the time history of a turn in which a 1.3g maneuver is initiated by an aileron step command, and the elevator is coordinated so that the result is a level turn. No rudder control or stability augmentation is used for the maneuver. It can be seen that the build-up in sideslip is negligible so that a rudder is unnecessary. The time to complete the maneuver, that is, to reach a steady-roll angle, is quite long since the inherently low damping in the Dutch roll oscillatory mode required small aileron input. Increasing the aileron input increases both the magnitude of the Dutch roll oscillation and the overshoot in roll angle.

Figure 27 also shows that the response time can be decreased considerably if stability augmentation in the form of a yaw damper is used. The angle of sideslip has increased but is still less than 1°. The damping gain was 4.36 radians per radian per second giving a maximum rudder deflection on the ventral fin of 17°.

CONCLUDING REMARKS

Longitudinal and lateral stability and control characteristics at subsonic speeds of a flat-top arrowhead wing-body combination have been determined from wind-tunnel tests and an analog computer study. It was found that the aerodynamic center moved forward by 10 percent of the mean aerodynamic chord as the lift coefficient was increased above 0.1. Although flown in the lift range of decreasing stability, the simulated airplane did not encounter pitch-up in maneuvers initiated from steady level flight with zero static margin unless a load factor of 2.2 was exceeded. This maneuver margin was provided by a large value of the pitching moment due to pitching velocity. To obtain zero static margin at trim lift, however, it was necessary to shift the center of gravity somewhat forward of the optimum location for maximum lift-drag ratio at hypersonic speeds. In the wind-tunnel tests the elevons and rudder maintained effectiveness at all angles of attack up to 22°.

The simulated airplane was stable in the Dutch roll mode but marginal in meeting military specifications for present-day aircraft. An analog study of the rolling maneuvers indicated that the simulated airplane was controllable with little lateral-longitudinal coupling even when unaugmented. With the addition of yaw damping, fairly rapid maneuvers could be executed with no serious overshoots or instabilities.

Ames Research Center
National Aeronautics and Space Administration
Moffett Field, Calif., Dec. 5, 1958

REFERENCES

1. Syvertson, Clarence A., Wong, Thomas J., and Gloria, Hermilo R.: Additional Experiments With Flat-Top Wing-Body Combinations at High Supersonic Speeds. NACA RM A56I11, 1957.

2. Syvertson, Clarence A., Gloria, Hermilo R., and Sarabia, Michael F.: Aerodynamic Performance and Static Stability and Control of Flat-Top Hypersonic Gliders at Mach Numbers From 0.6 to 18. NACA RM A58G17, 1958.

3. Beam, Benjamin H.: A Wind-Tunnel Technique for Measuring the Dynamic Rotary Stability Derivatives at Subsonic and Supersonic Speeds. NACA Rep. 1258, 1956. (Supersedes NACA TN 3347)

4. Buell, Donald A., and Tinling, Bruce E.: Ground Effects on the Longitudinal Characteristics of Two Models With Wings Having Low Aspect Ratio and Pointed Tips. NACA TN 4044, 1957. (Supersedes NACA RM A55E04)

5. Herriot, John G.: Blockage Corrections for Three-Dimensional-Flow Closed Throat Wind Tunnels, With Consideration of the Effect of Compressibility. NACA Rep 995, 1950. (Supersedes NACA RM A7B28)

6. Sivells, James C., and Salmi, Rachel M.: Jet-Boundary Corrections For Complete and Semispan Swept Wings in Closed Circular Wind Tunnels. NACA TN 2454, 1951.

7. Weber, J.: Some Effects of Flow Separation on Slender Delta Wings. R.A.E. TN Aero. 2425 (British), 1955.

8. Kelly, Mark W.: Wind-Tunnel Investigation of the Low-Speed Aerodynamic Characteristics of a Hypersonic Glider Configuration. NACA RM A58F03, 1958.

9. Anon.: Flying Qualities of Piloted Airplanes. U. S. Air Force Spec., MIL-F-8785 (ASG), Sept. 1, 1954. (Amendment I, Oct. 19, 1954; Amendment II, Oct. 17, 1955)

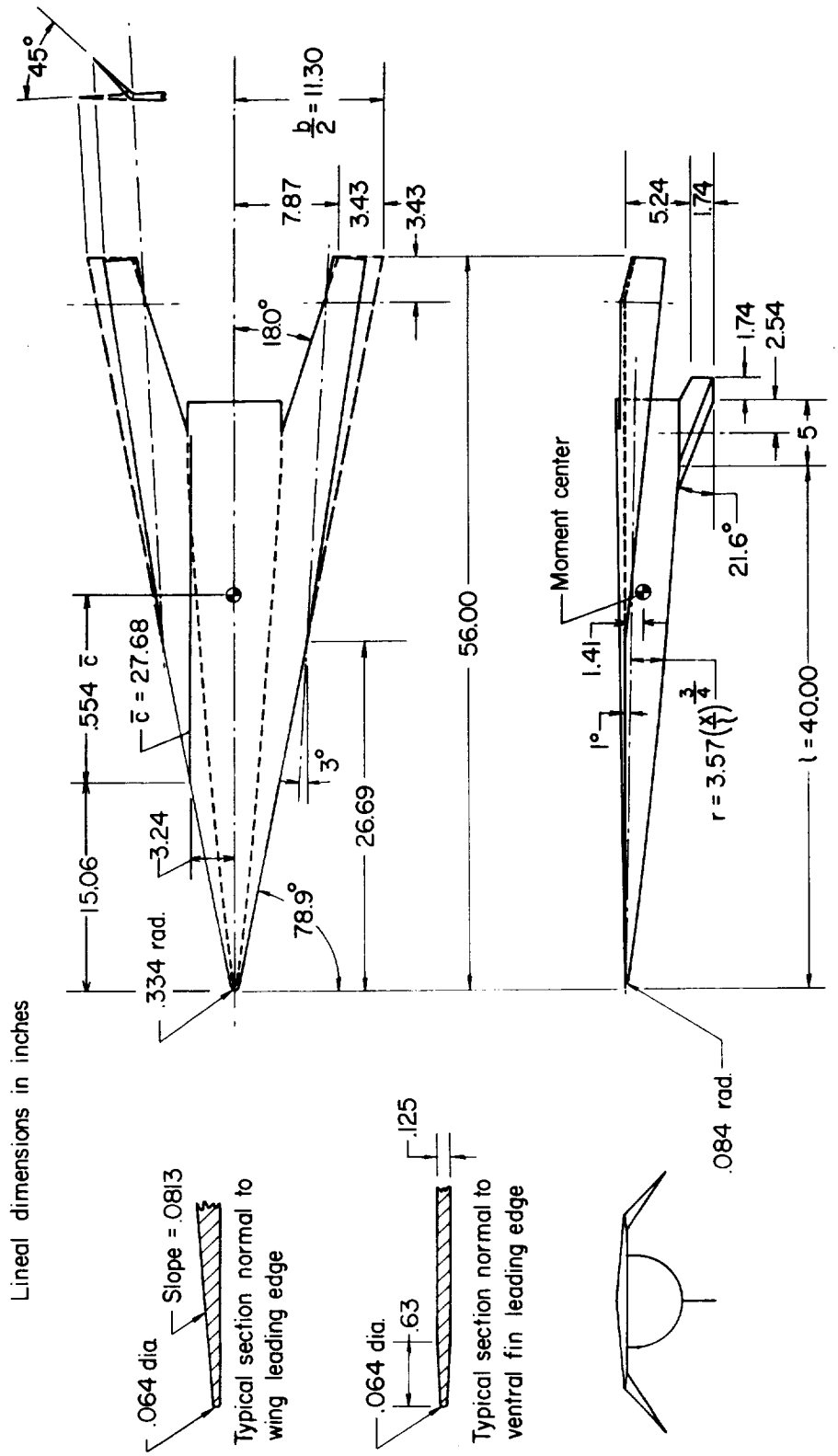

(a) Geometry of the model.

Figure 1.- The model.

A-23044

(b) Model mounted in the wind tunnel over the ground plate.

Figure 1.- Concluded

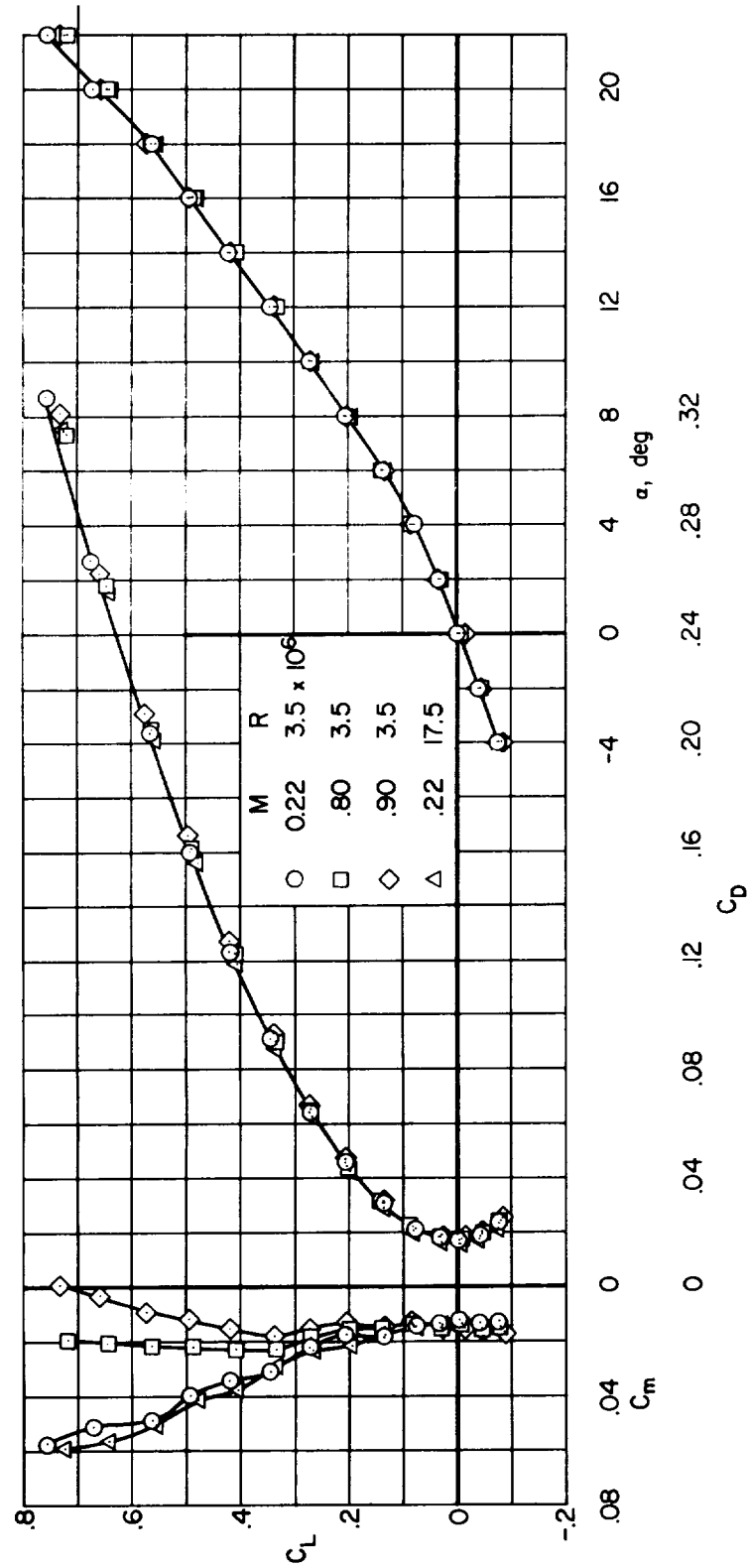

Figure 2.- The static longitudinal characteristics of the model; control surfaces neutral, moment center at 0.55$\bar{c}$.

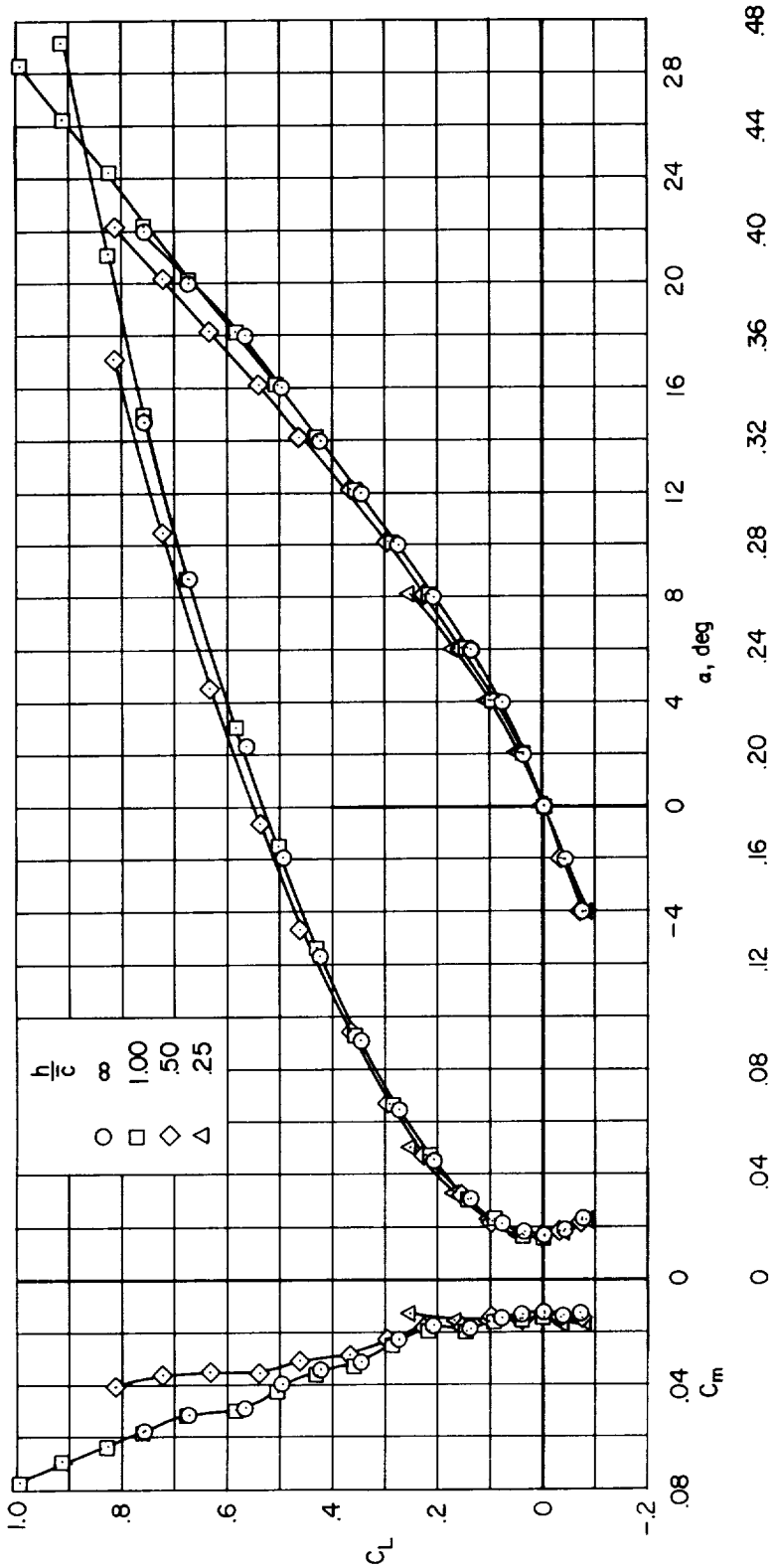

Figure 3.- The effects of ground proximity on the static longitudinal characteristics of the model; ventral fin off, control surfaces neutral, M = 0.22, moment center at 0.55$\bar{c}$.

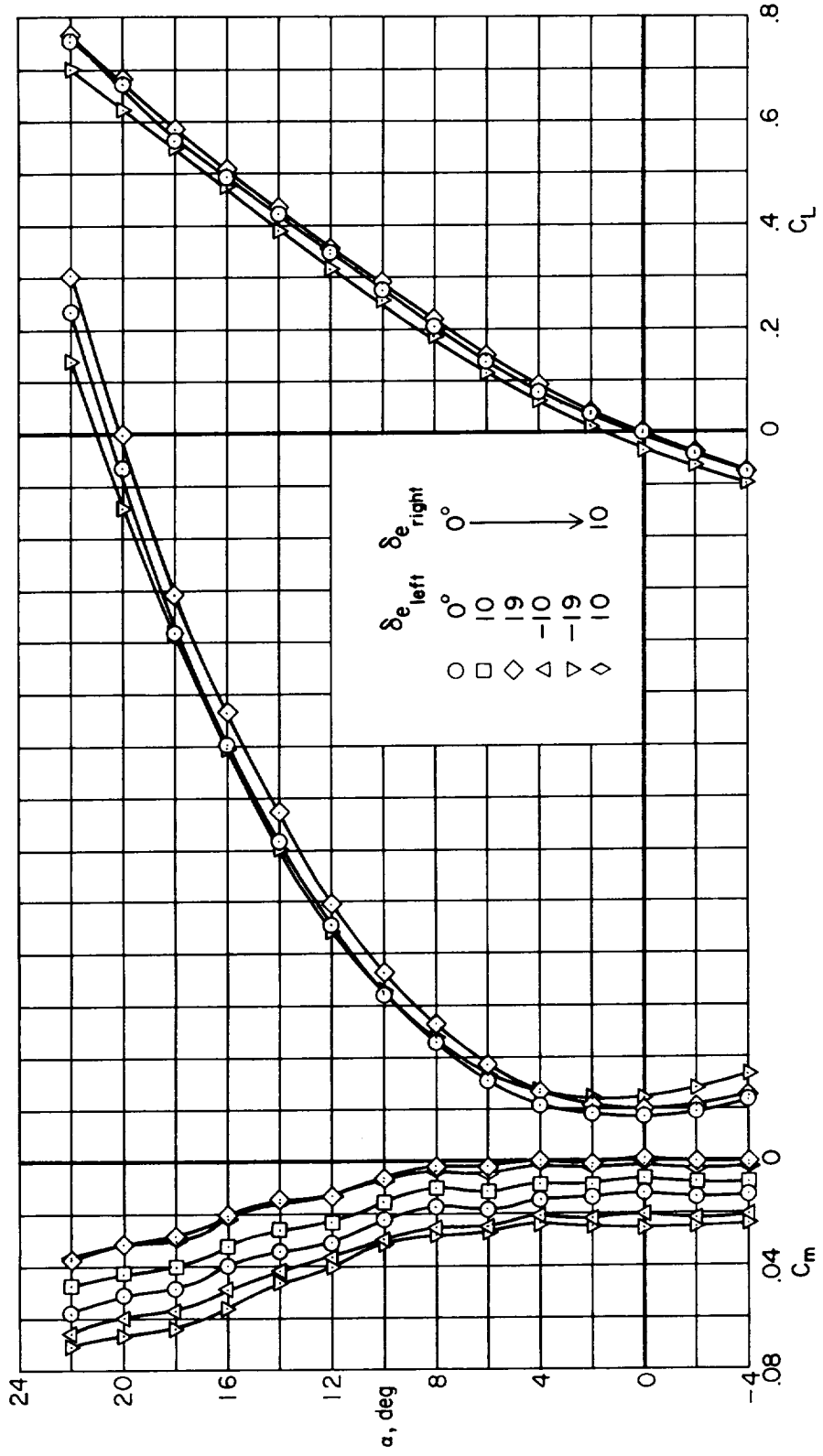

Figure 4.- The static longitudinal characteristics of the model; M = 0.22, moment center at 0.55$\bar{c}$.

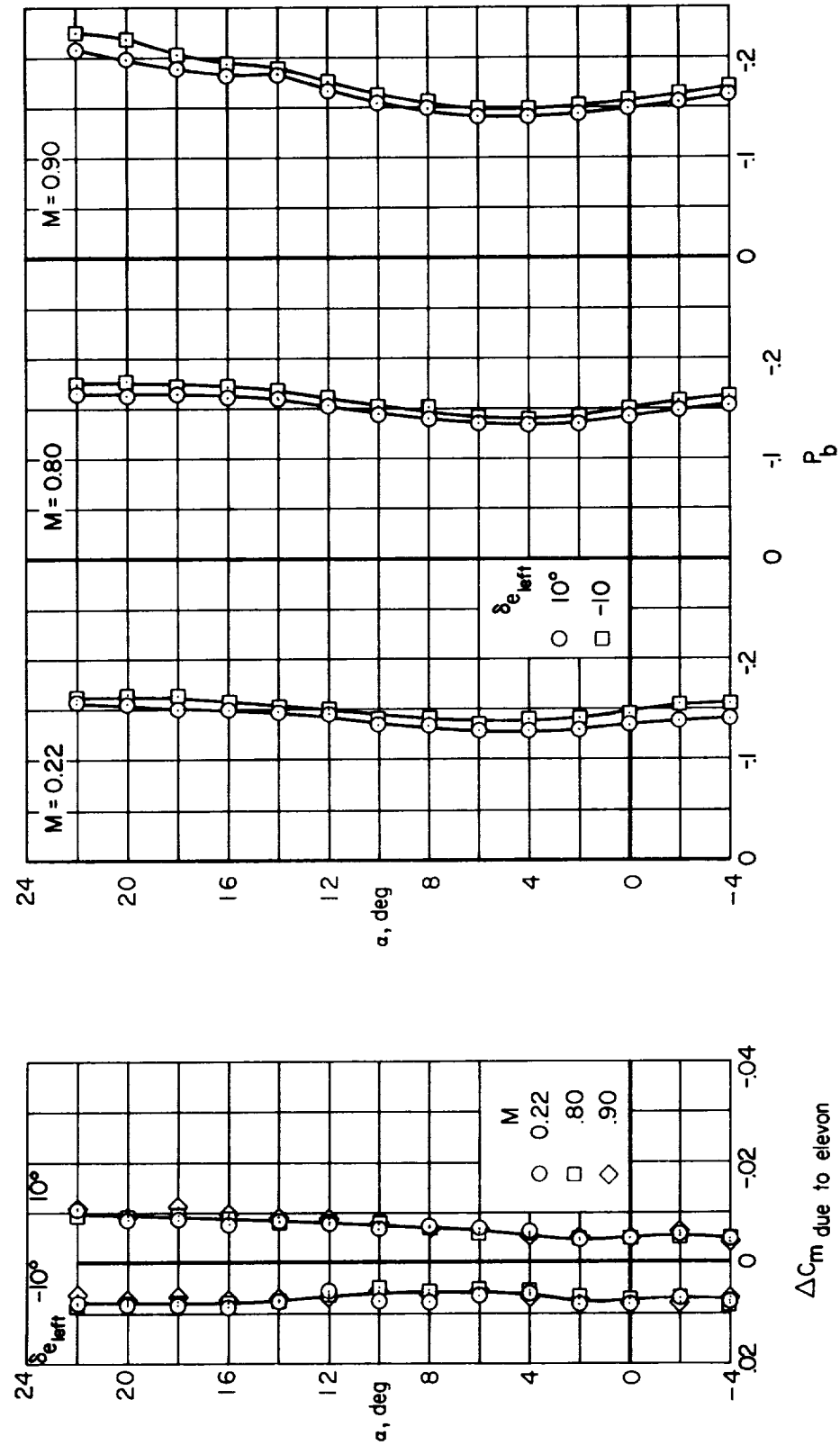

Figure 5.- The effect of Mach number on the incremental pitching-moment coefficients due to elevon deflection, and the base pressure coefficients of the model; moment center at $0.55\bar{c}$.

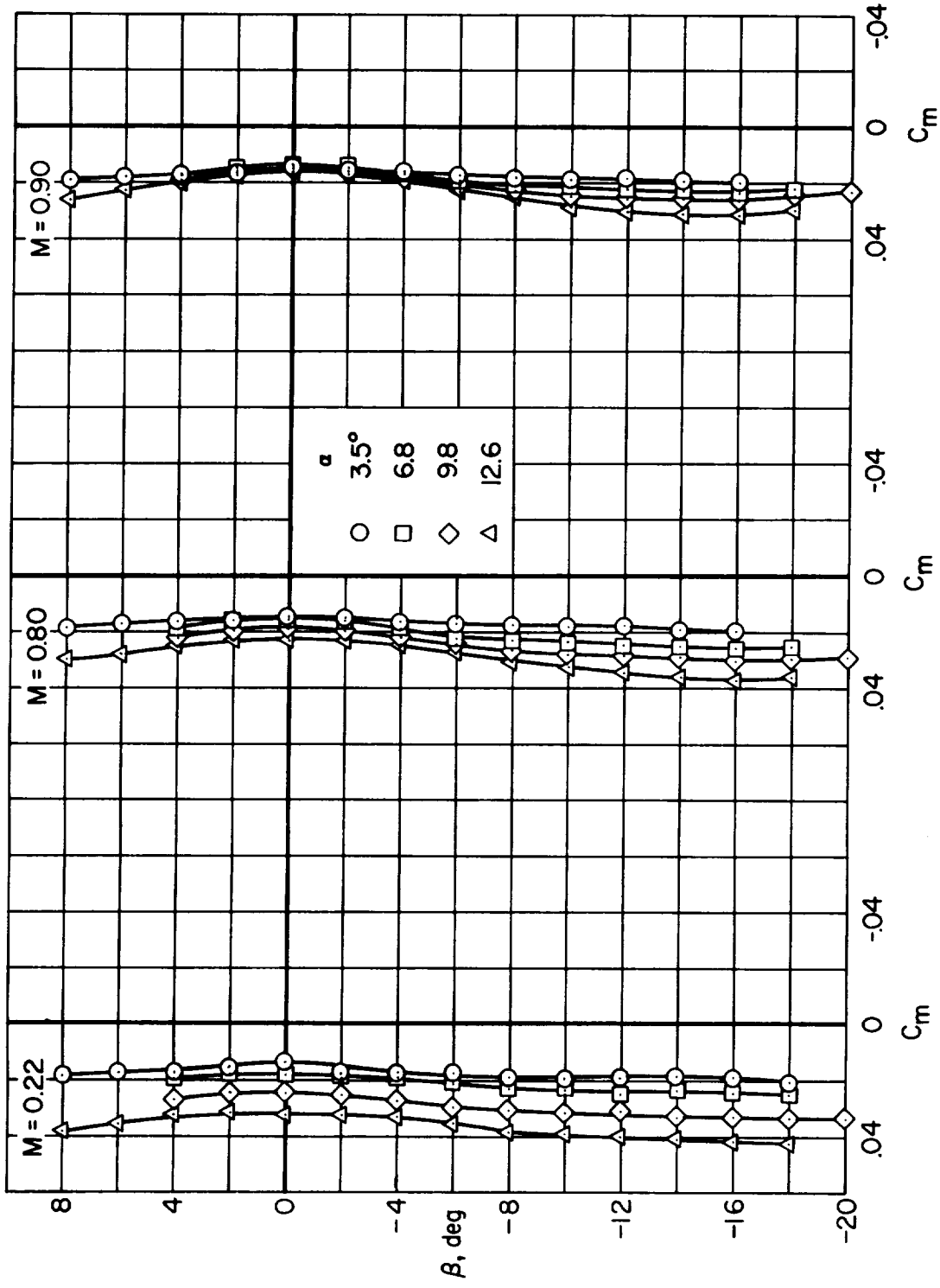

Figure 6.- The effect of sideslip angle on the pitching-moment coefficients of the model; control surfaces neutral, moment center at 0.55$\bar{c}$.

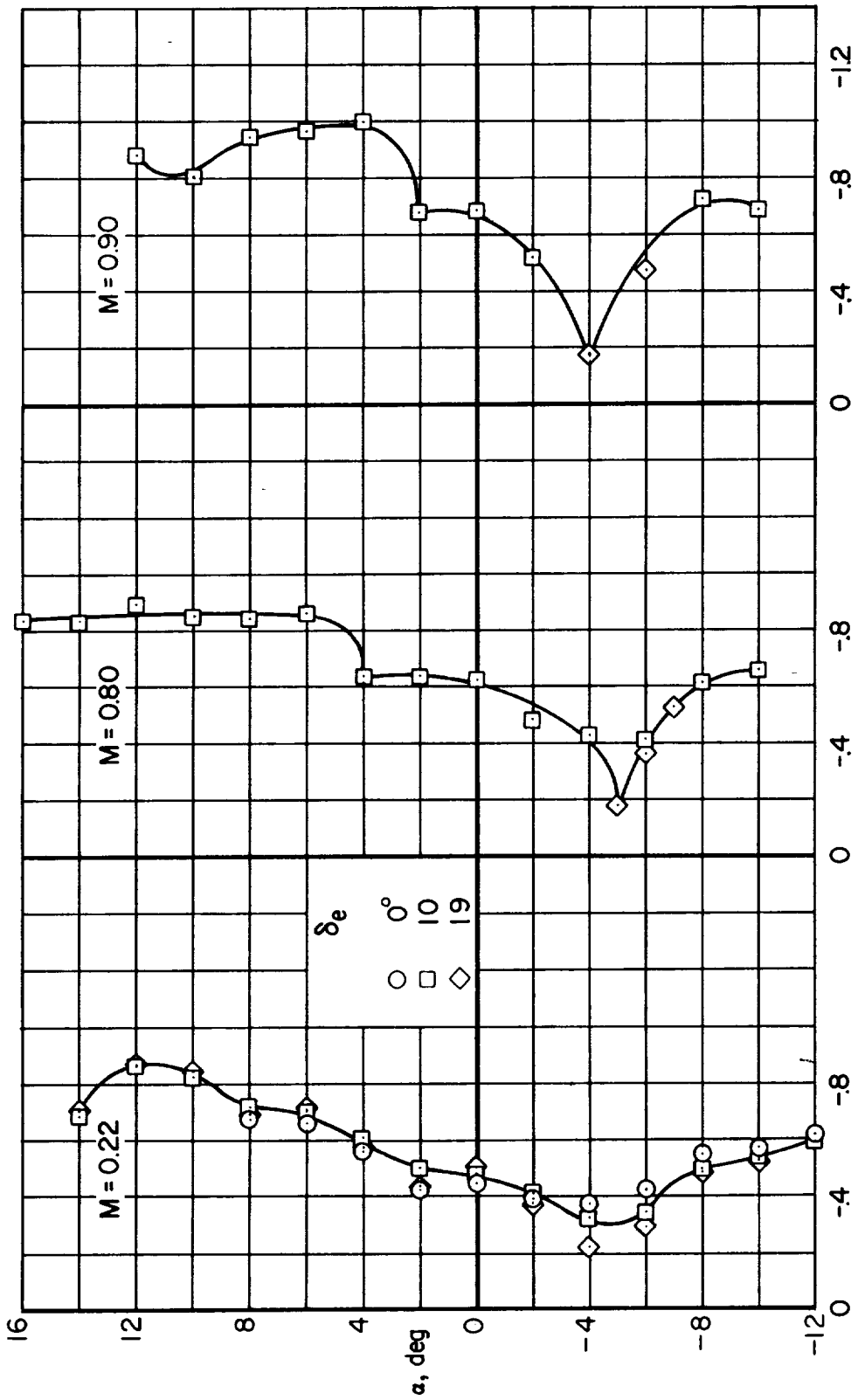

Figure 7.- The damping in pitch of the model; moment center at 0.55$\bar{c}$.

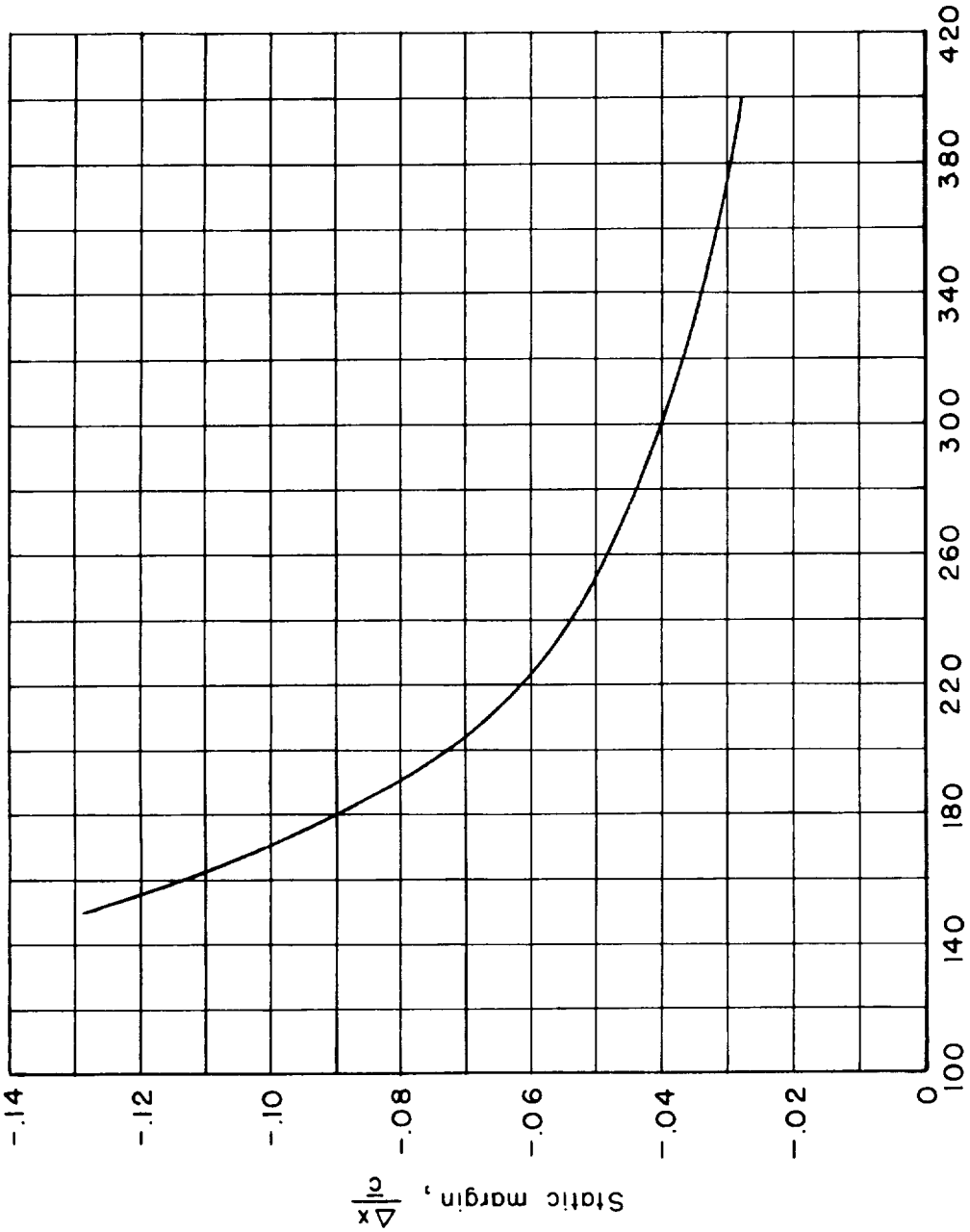

Figure 8.- The variation of static margin with velocity for the simulated airplane; center of gravity at 0.55$\bar{c}$.

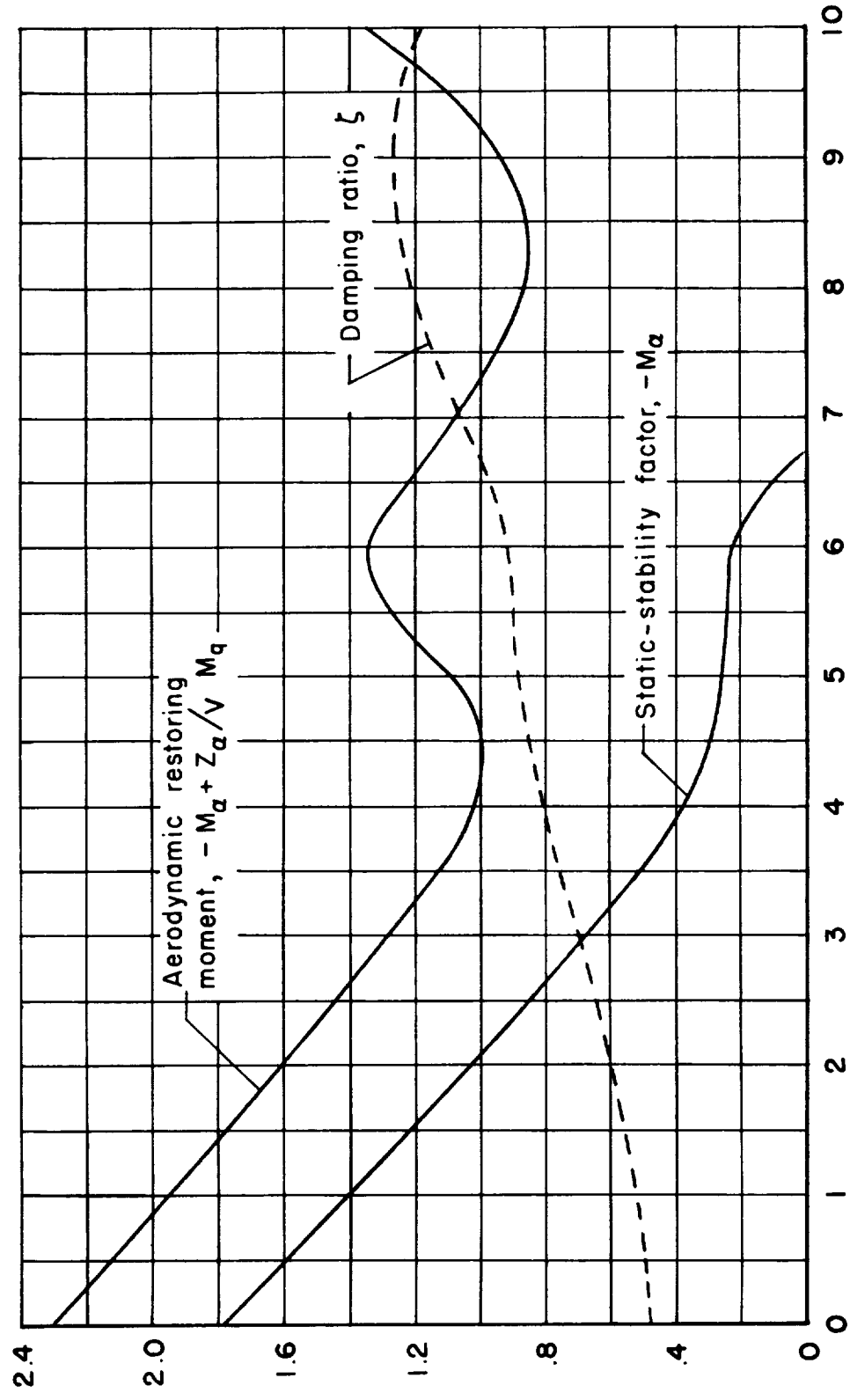

Figure 9.- Comparison of static stability and aerodynamic restoring moment for the simulated airplane; V = 300 feet per second, center of gravity at 0.51$\bar{c}$.

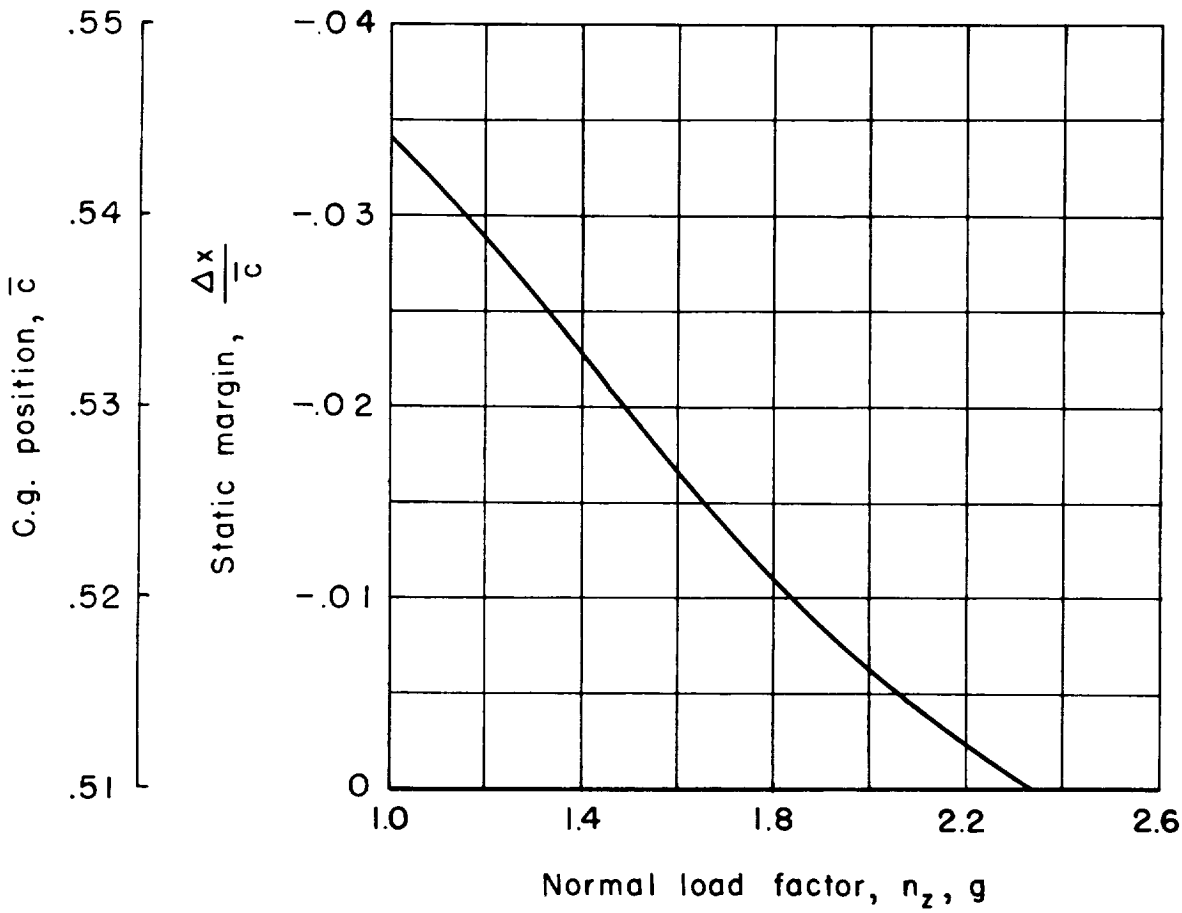

Figure 10.- The static margin for stability in pull-ups of the simulated airplane; V = 300 feet per second.

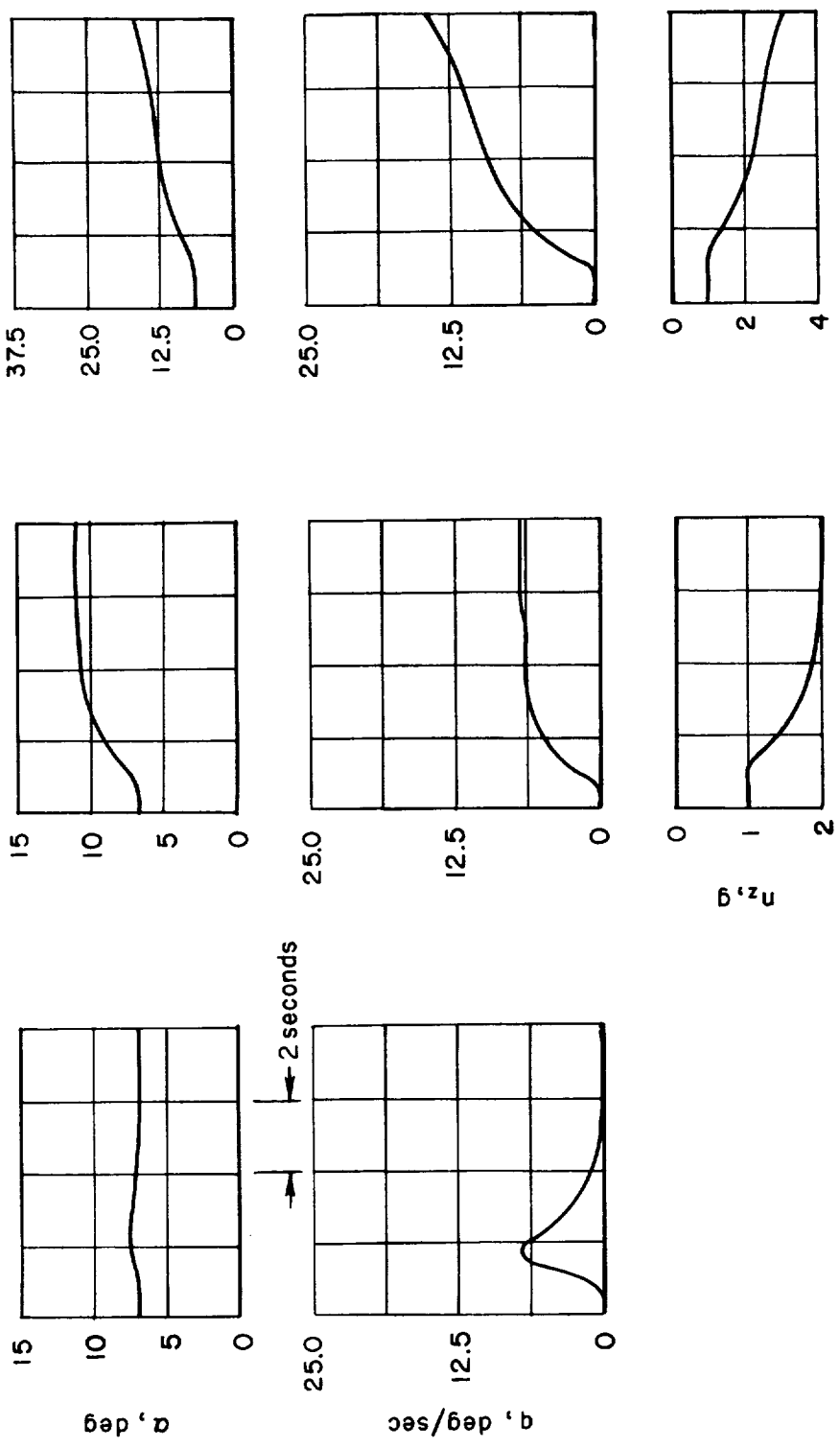

Figure 11.- Longitudinal response of the simulated airplane for zero static margin; V = 300 feet per second, center of gravity at 0.51$\bar{c}$.

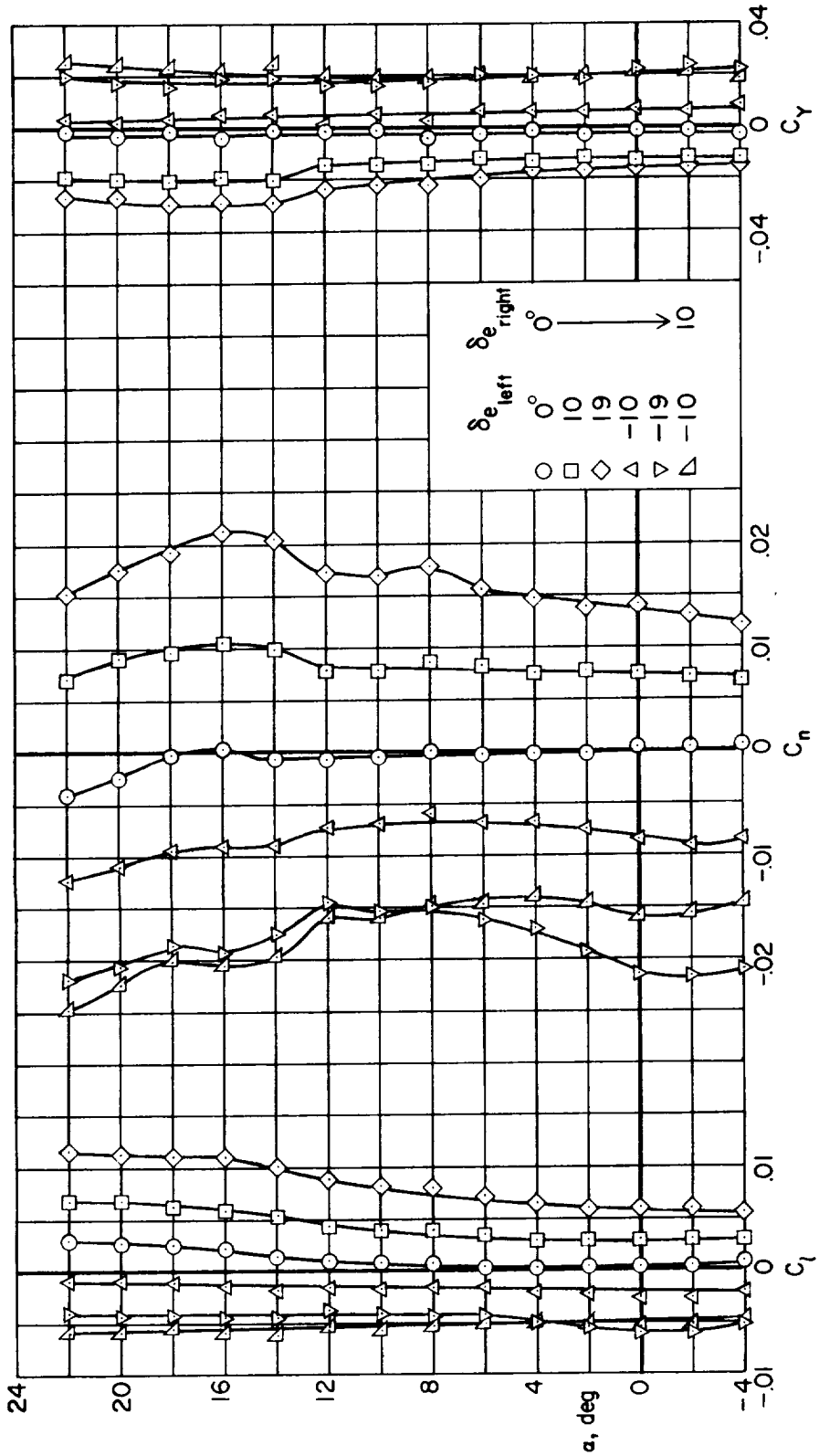

(a) Deflection of elevons.

Figure 12.- The effects of control-surface deflection on the rolling-moment, yawing-moment, and side-force coefficients of the model; $\beta = 0^{\circ}$, M = 0.22.

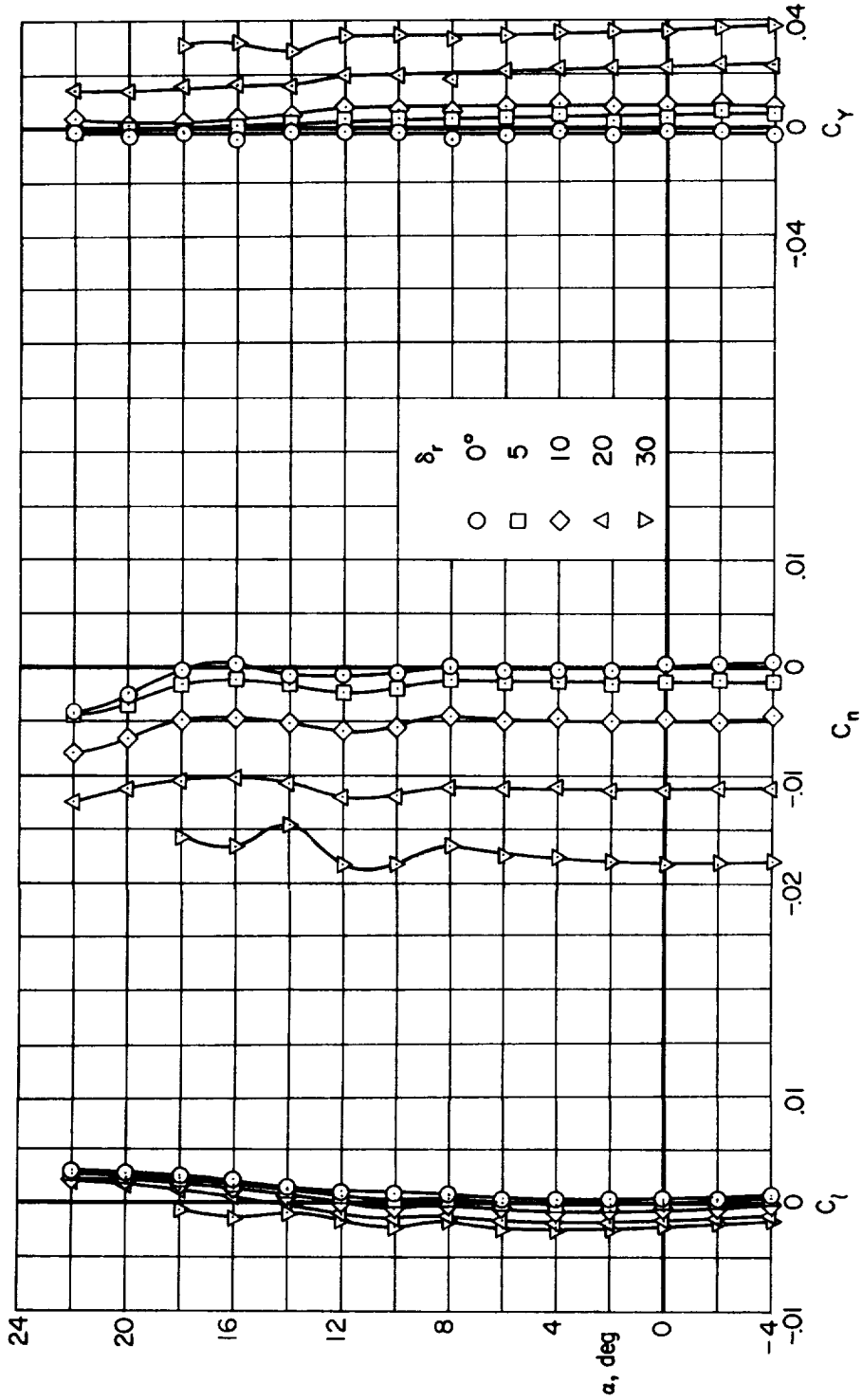

(b) Deflection of rudder.

Figure 12.- Continued.

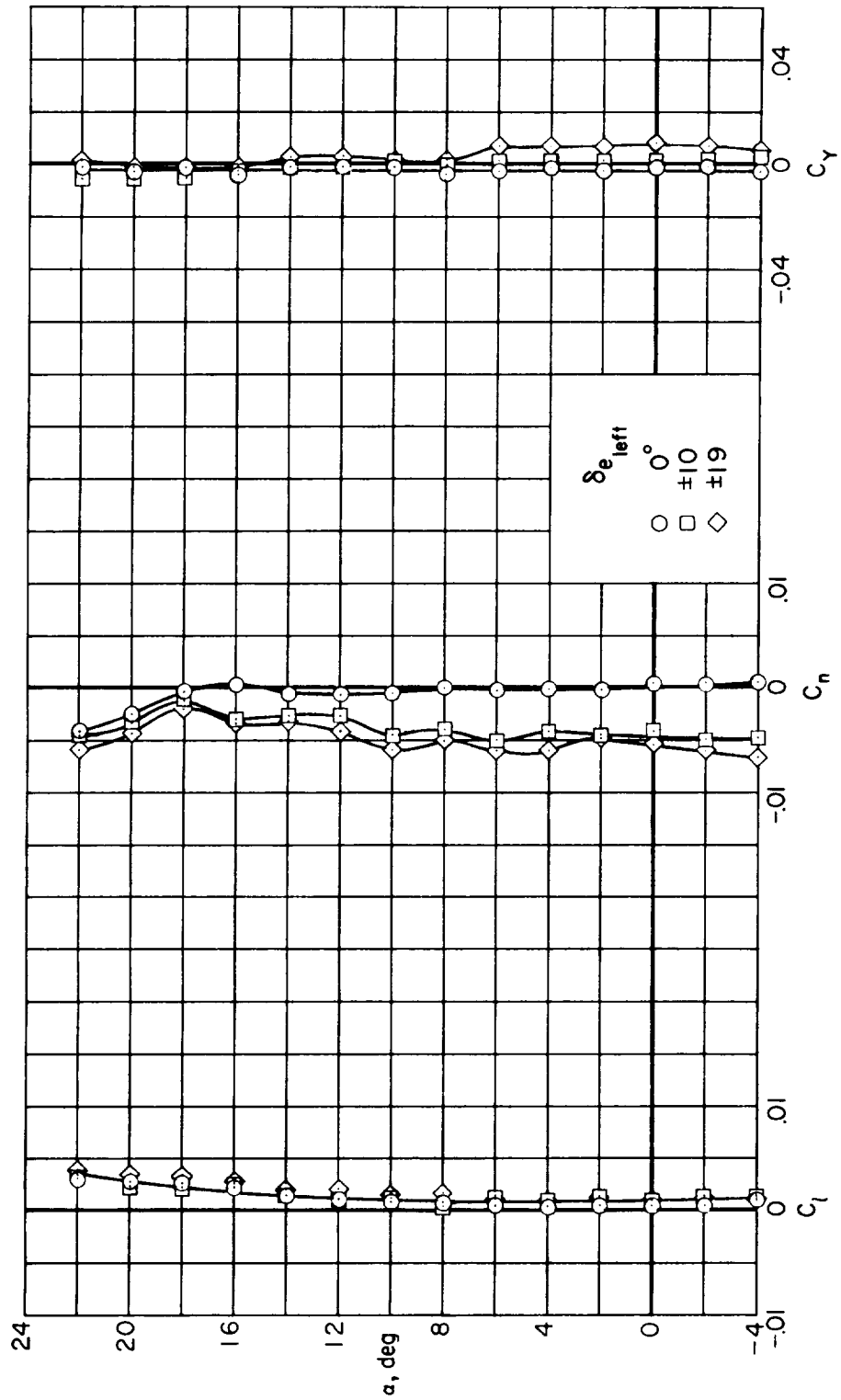

(c) Deflection of split-flap type elevon.

Figure 12.- Concluded.

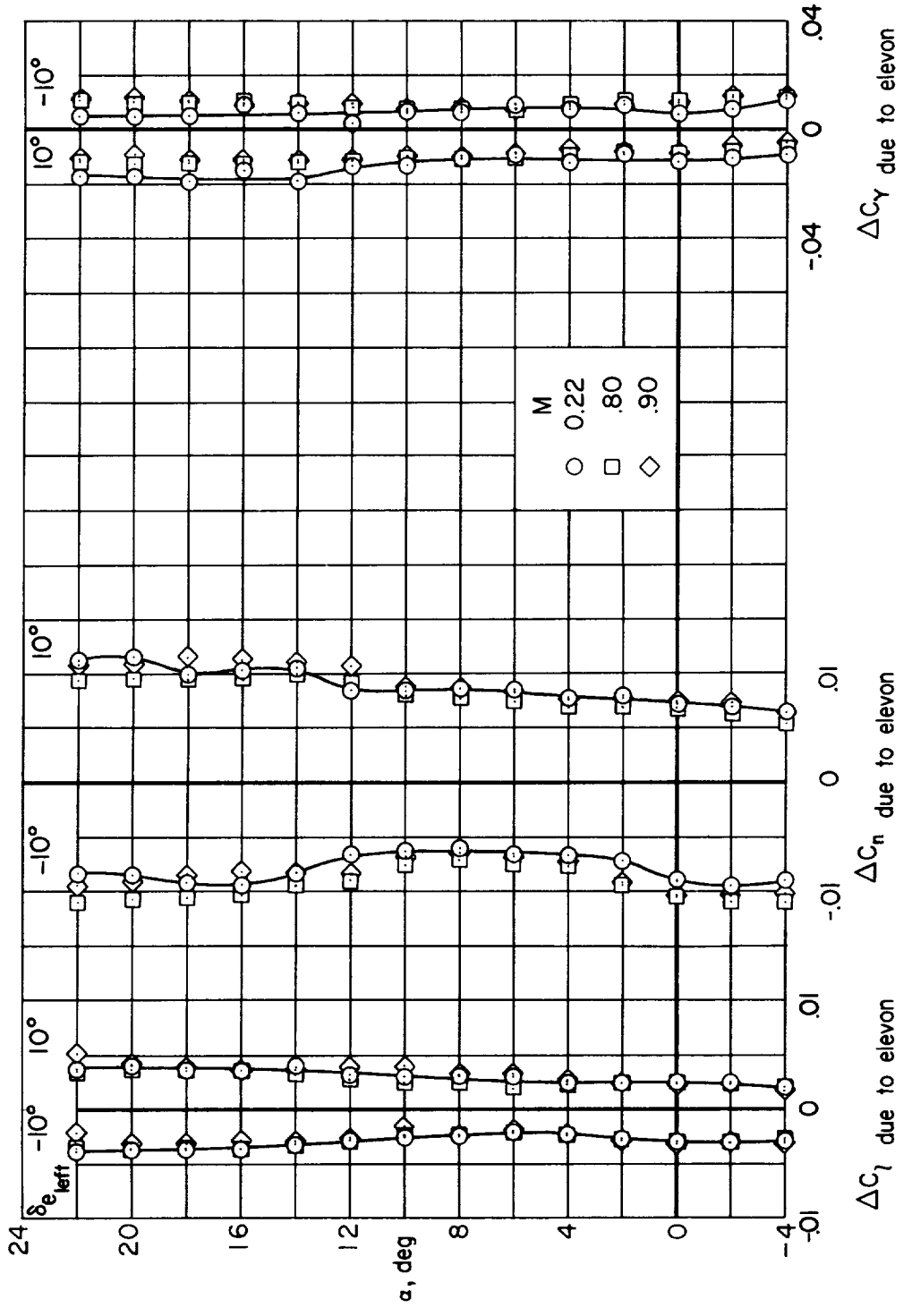

(a) Deflection of elevon.

Figure 13.- The effects of Mach number on the incremental rolling-moment, yawing-moment, and side-force coefficients due to control-surface deflection; $\beta = 0°$.

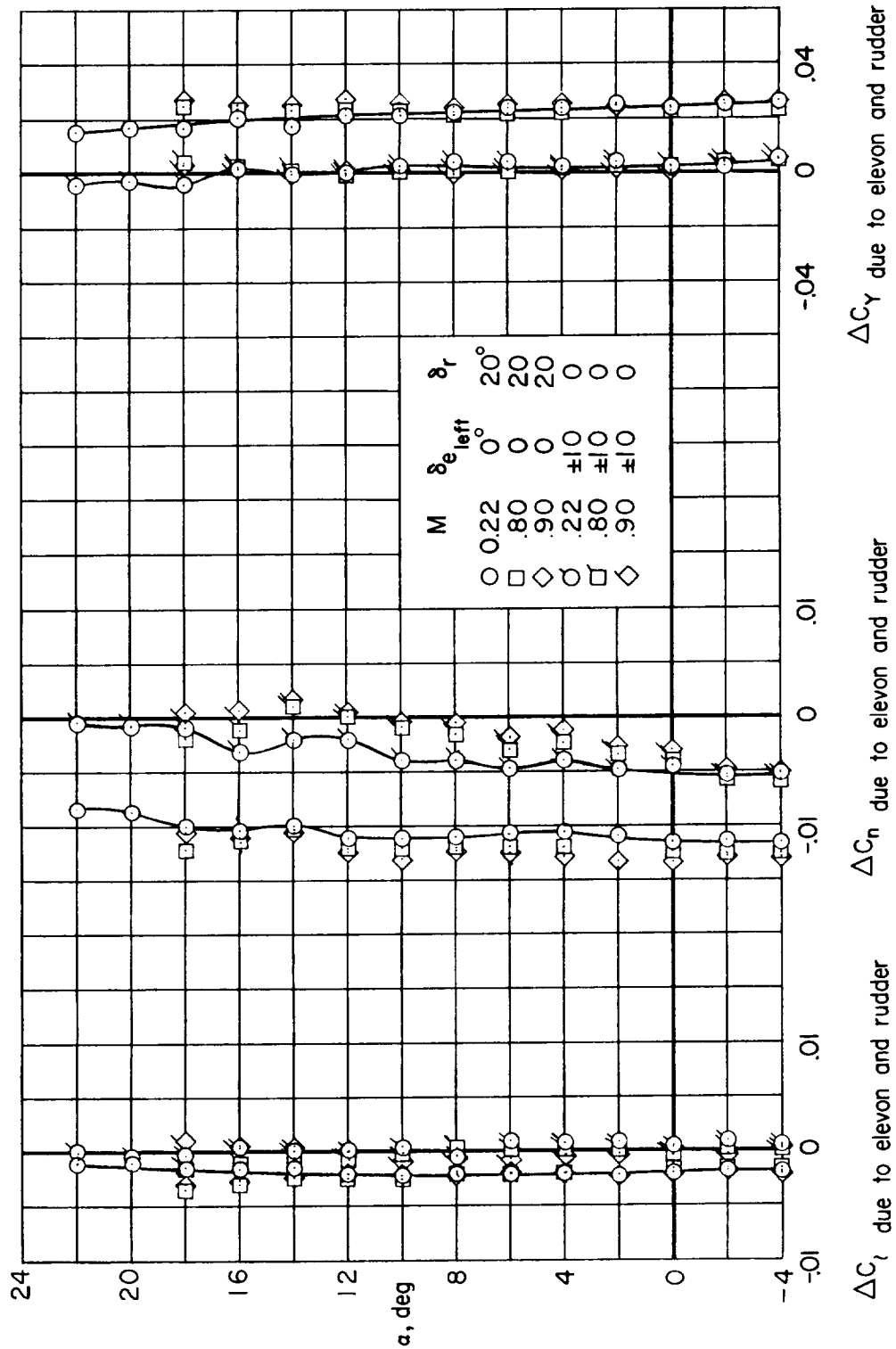

(b) Deflection of rudder and split-flap type elevon.

Figure 13.- Concluded.

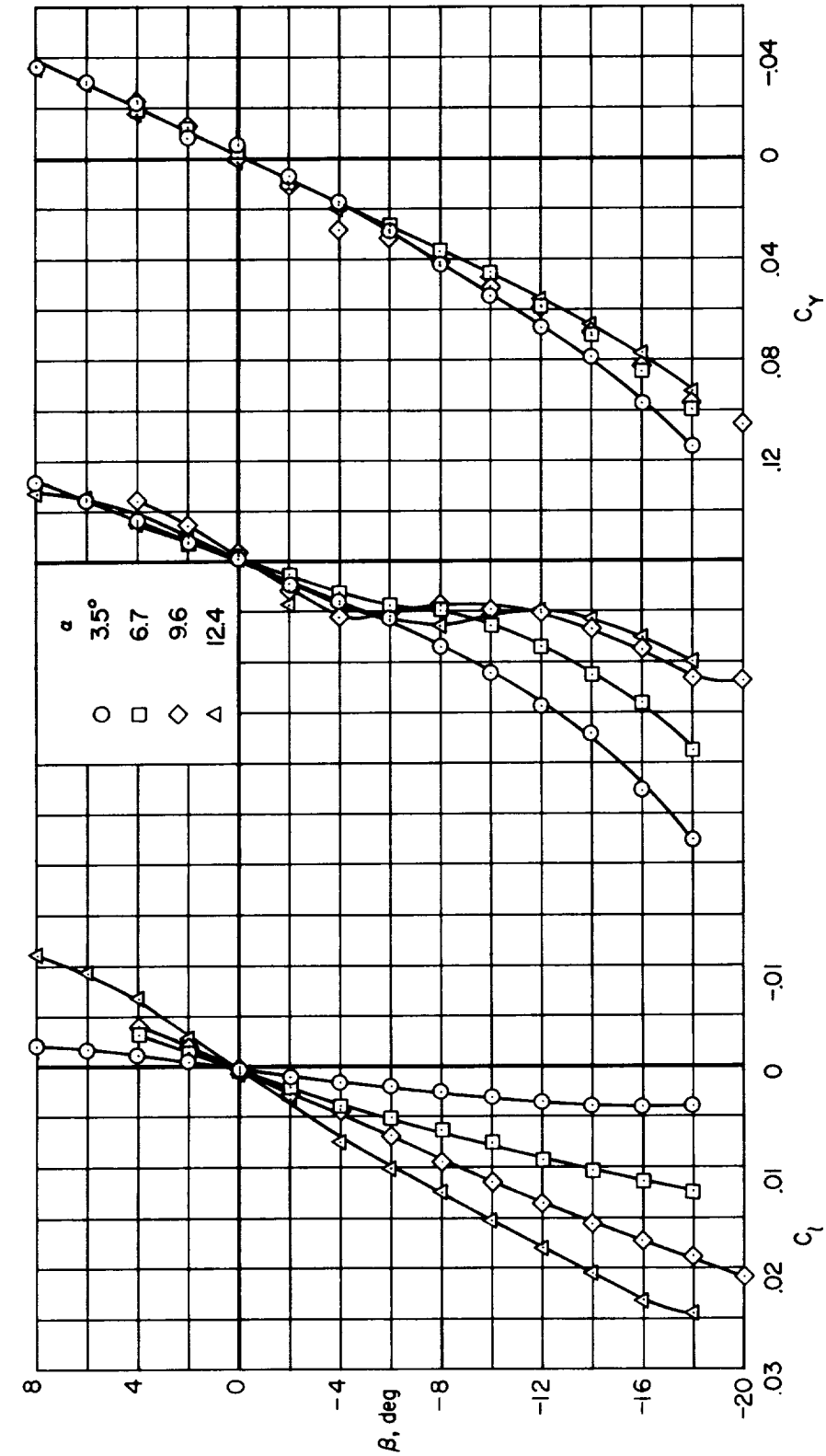

(a) M = 0.22

Figure 14.- The static lateral and directional characteristics of the model; control surfaces neutral.

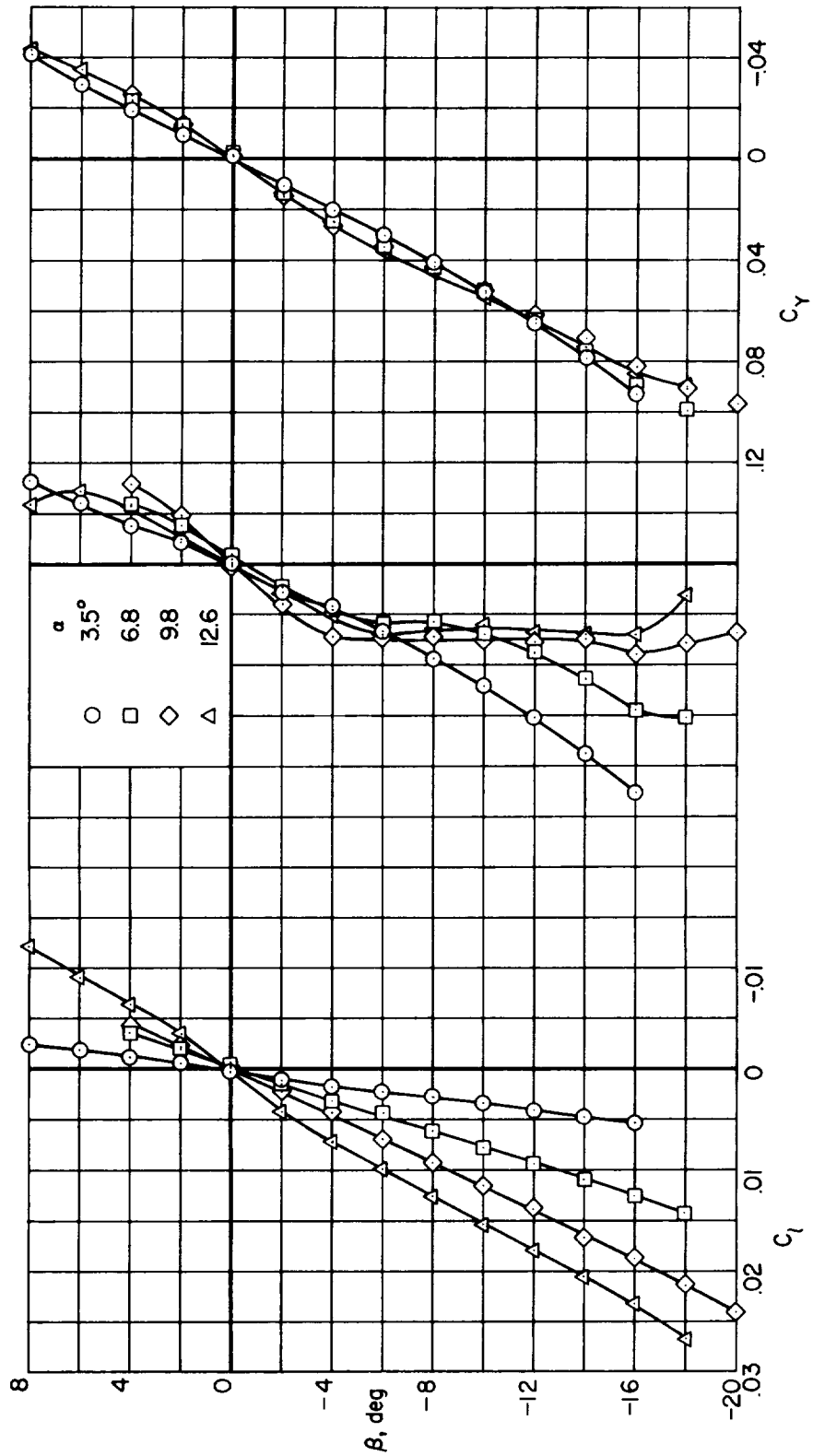

(b) M = 0.80

Figure 14.- Continued.

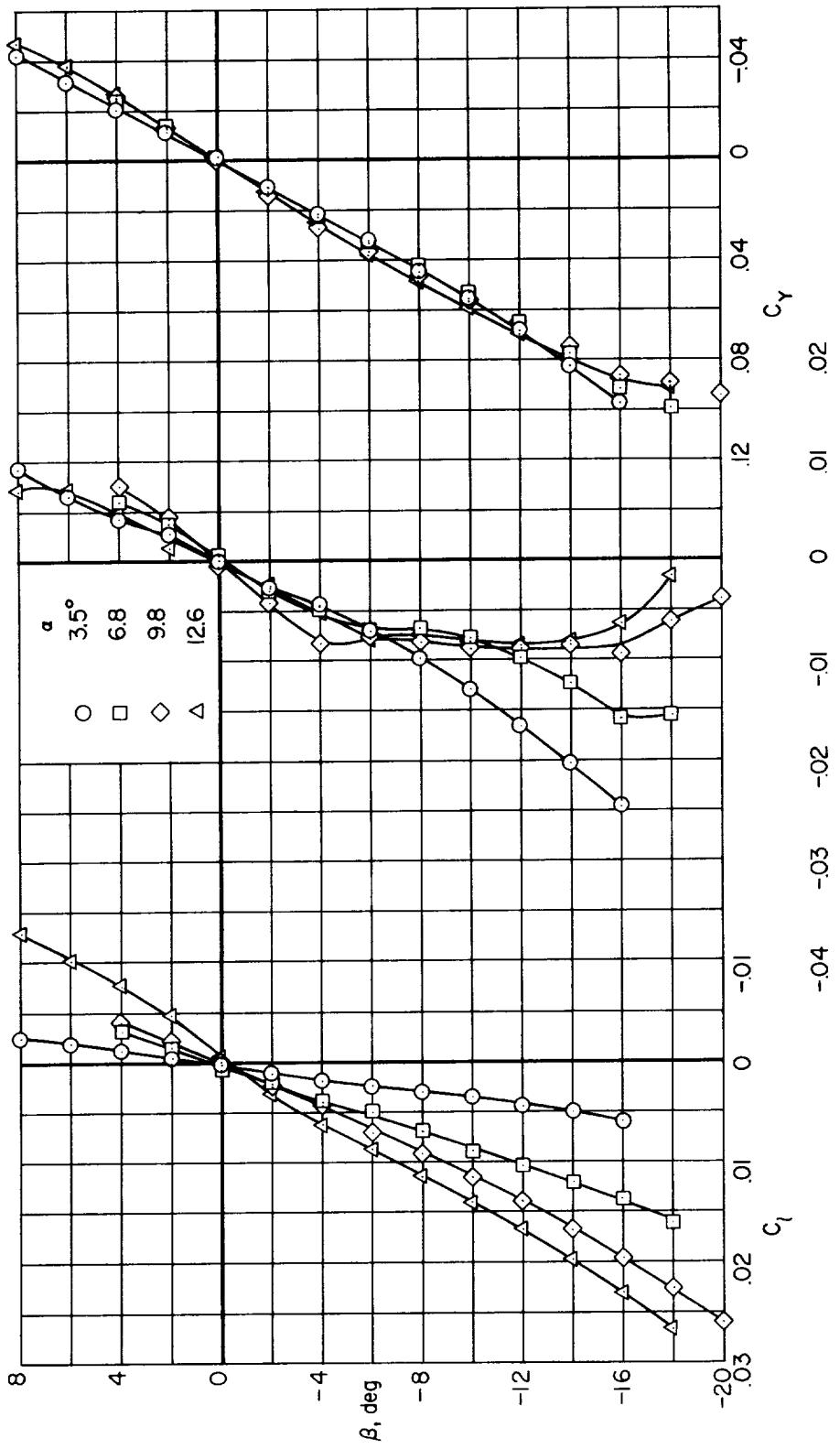

(c) M = 0.90

Figure 14.- Concluded.

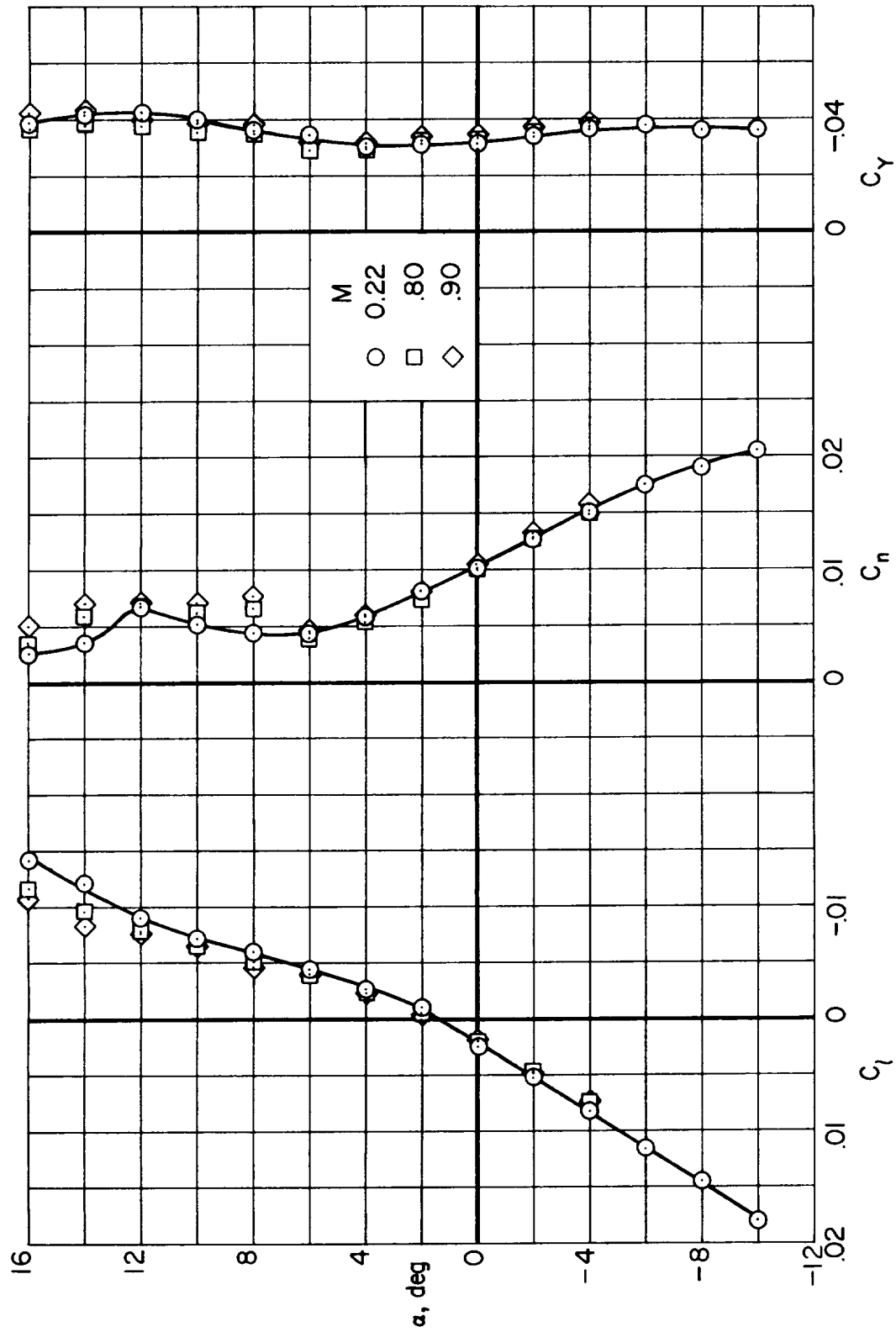

Figure 15.- The variation of rolling-moment, yawing-moment, and side-force coefficients of the model with angle of attack; control surfaces neutral, $\beta = 6^{\circ}$.

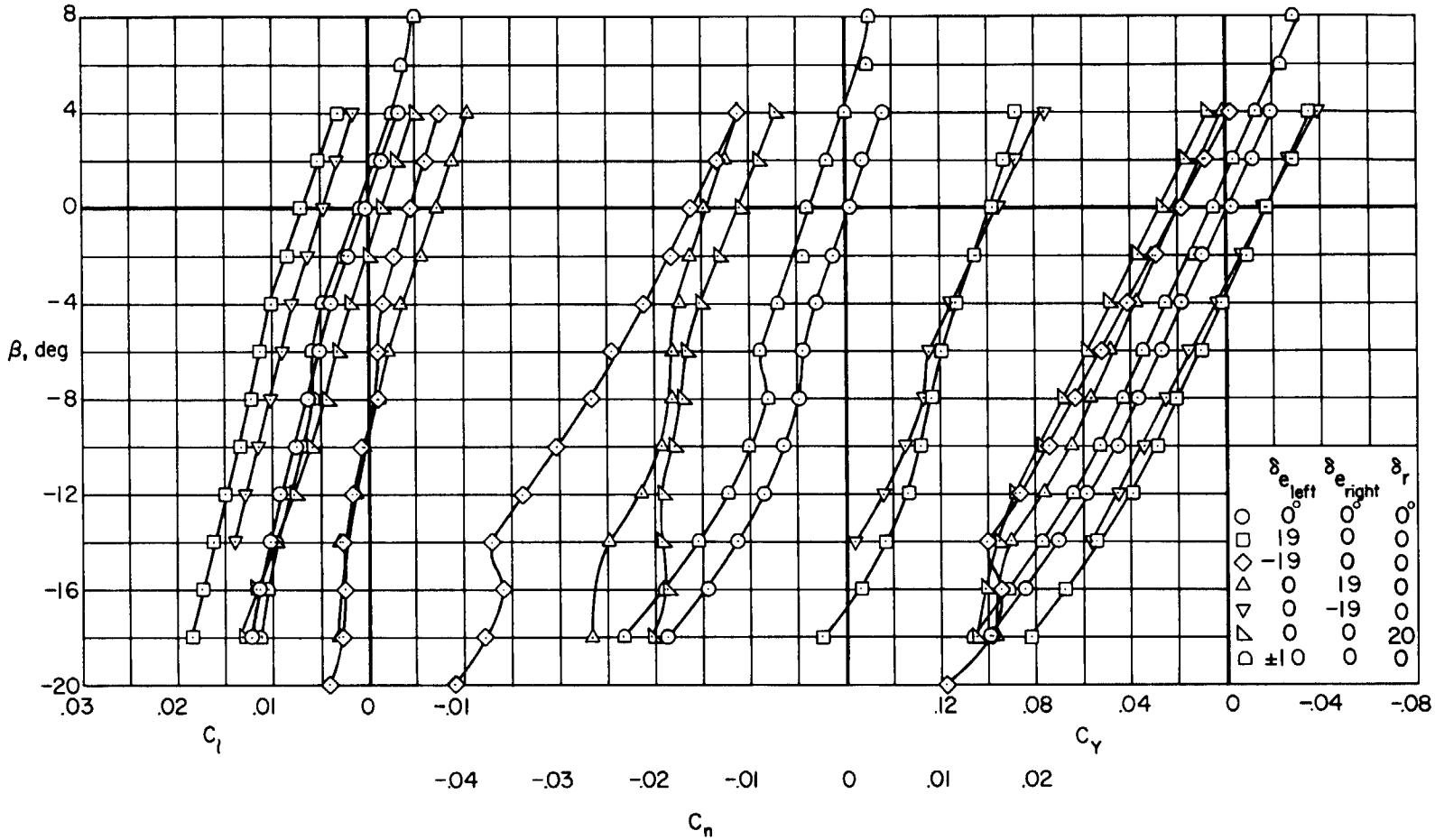

(a) $\alpha = 6.7^\circ$

Figure 16.- The effects of control-surface deflection on the static lateral and directional characteristics of the model; M = 0.22.

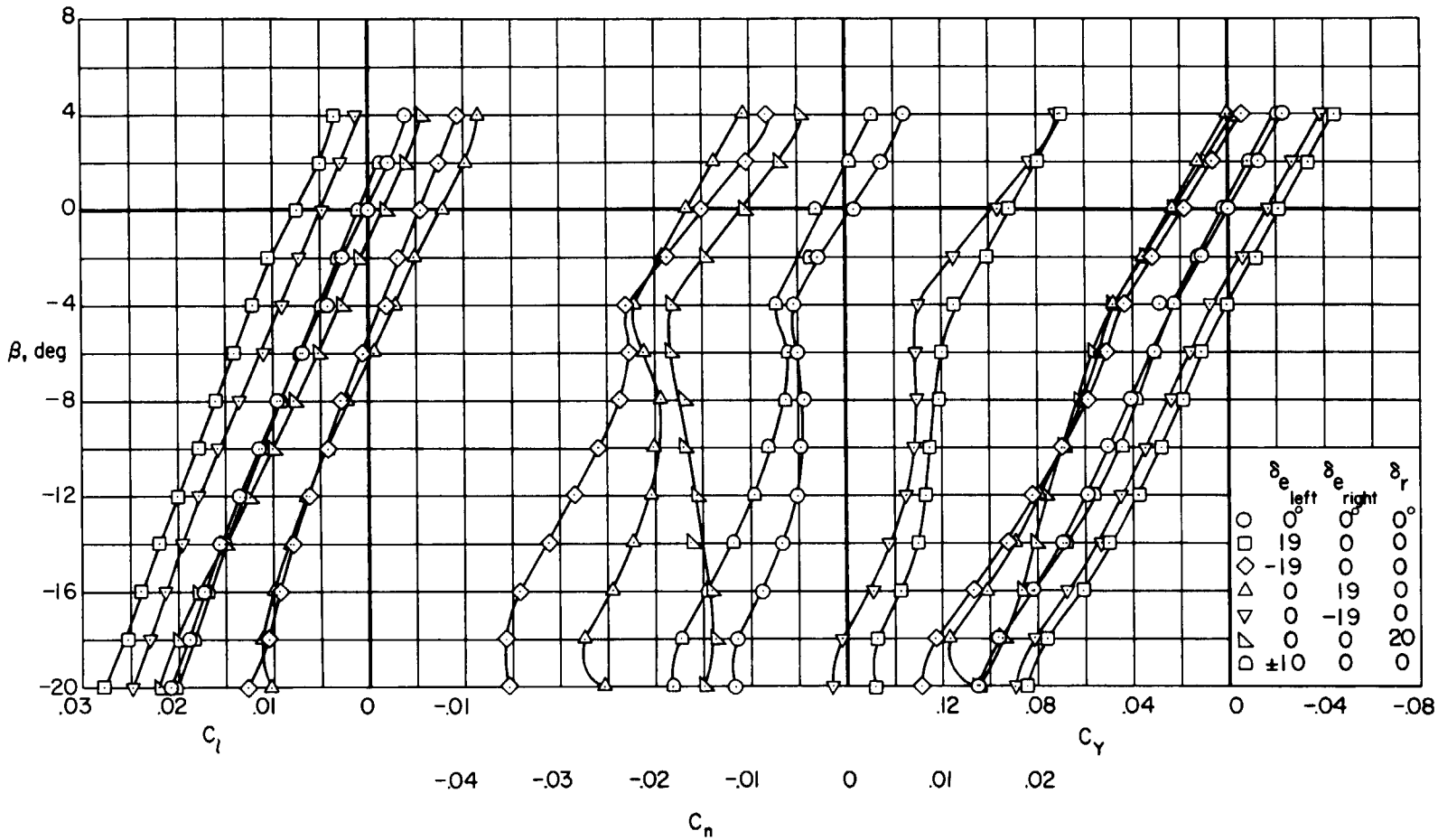

(b) $\alpha = 9.6^{\circ}$

Figure 16.- Concluded.

Figure 17.- The lateral rotary stability derivatives of the model; $\beta \cong 0^{\circ}$.

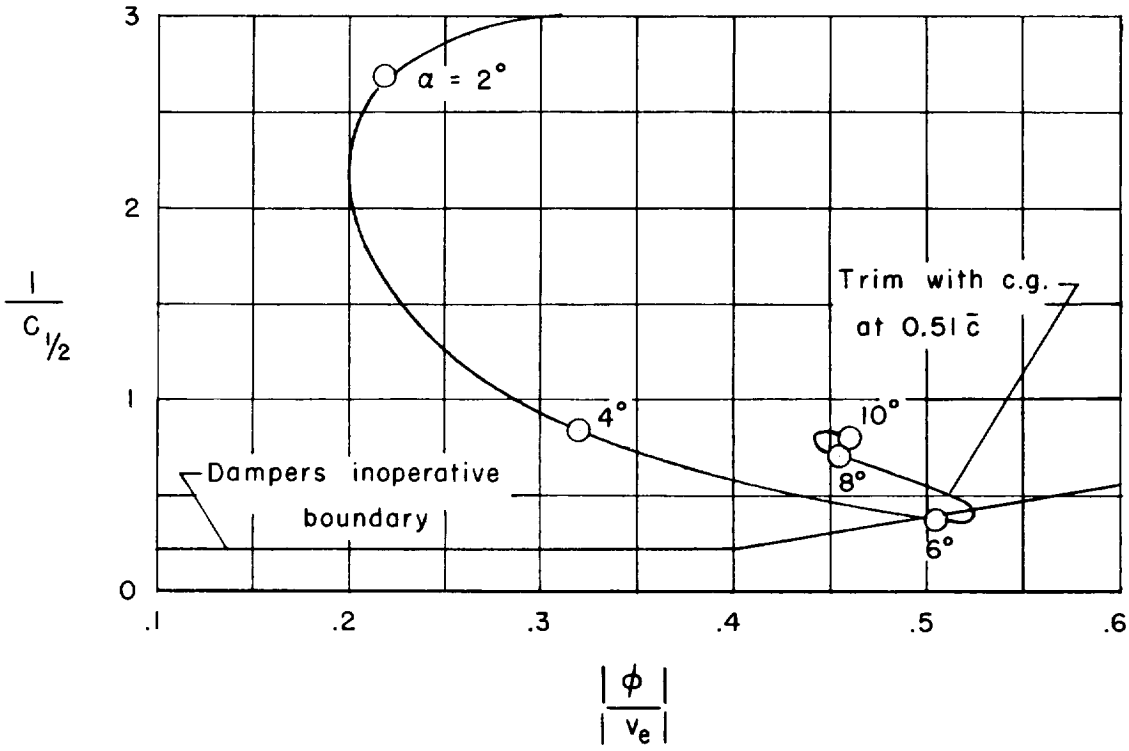

Figure 18.- Dutch roll characteristics of the simulated airplane; V = 300 feet per second.

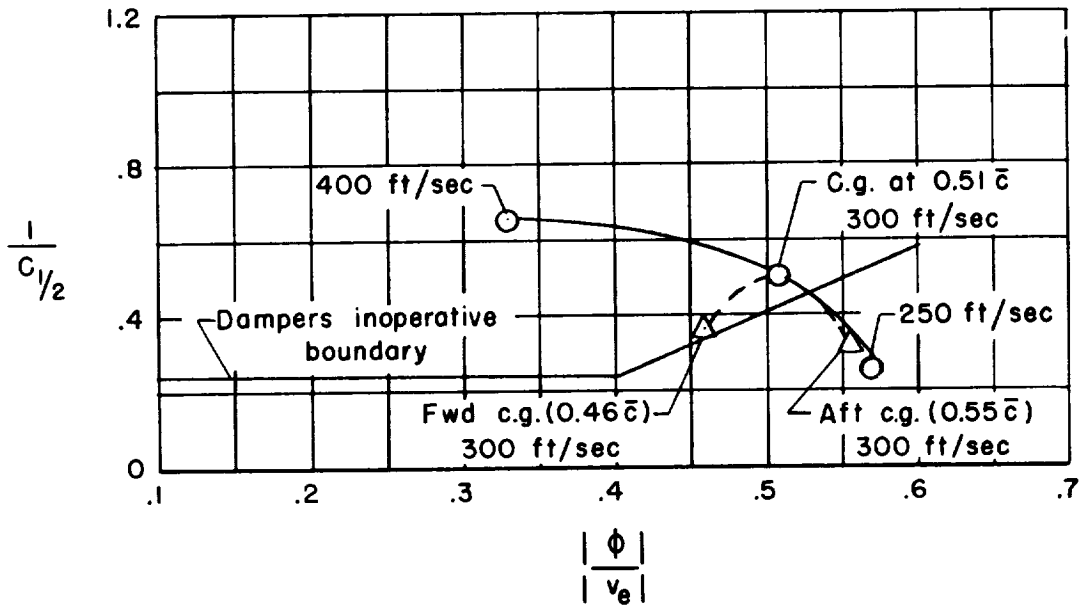

Figure 19.- Dutch roll characteristics of the simulated airplane for several center of gravity positions and landing velocities at trim angle of attack.

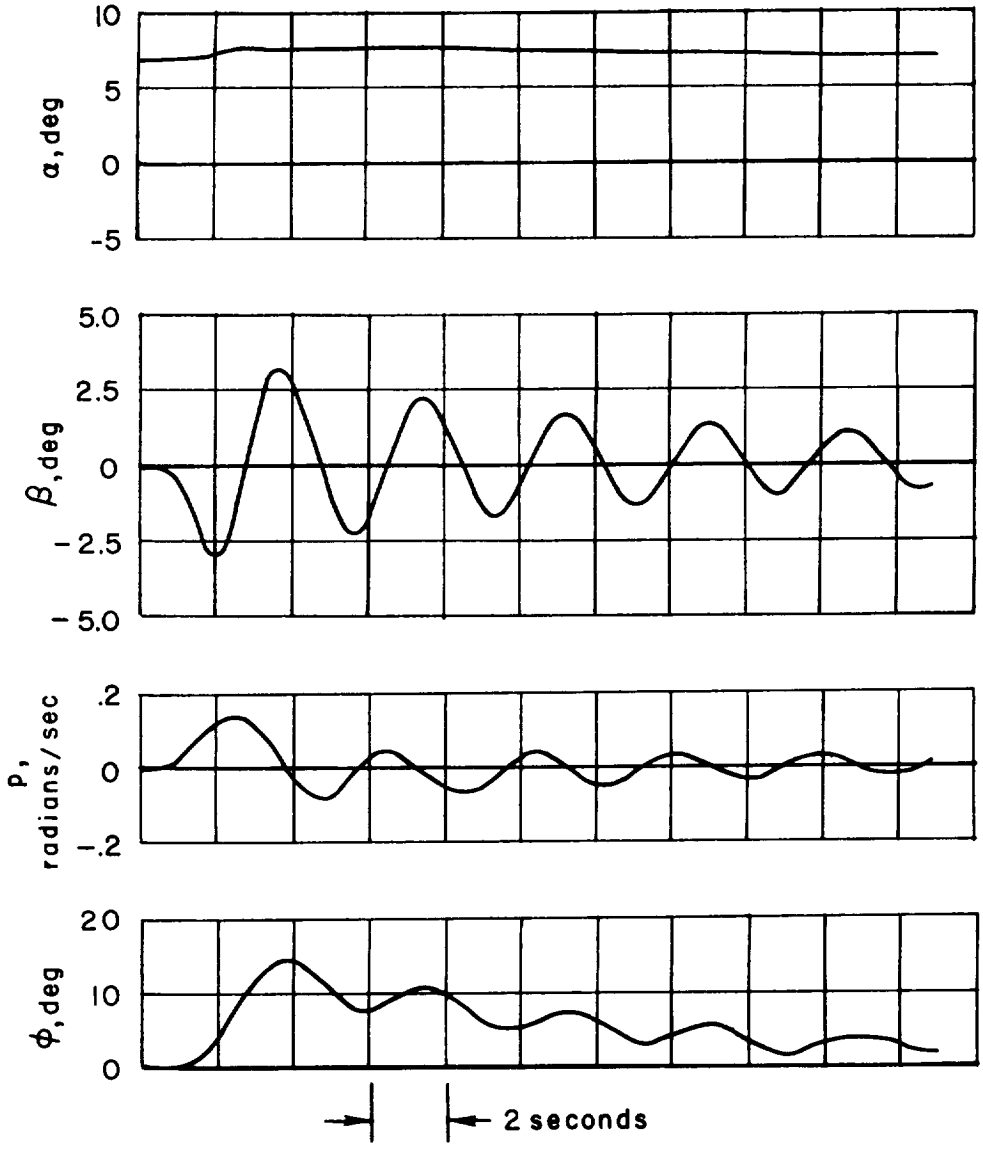

Figure 20.- Response of the simulated airplane to a rudder pulse; $\alpha_{trim} = 6.9^{\circ}$, V = 300 feet per second, center of gravity at $0.51\bar{c}$.

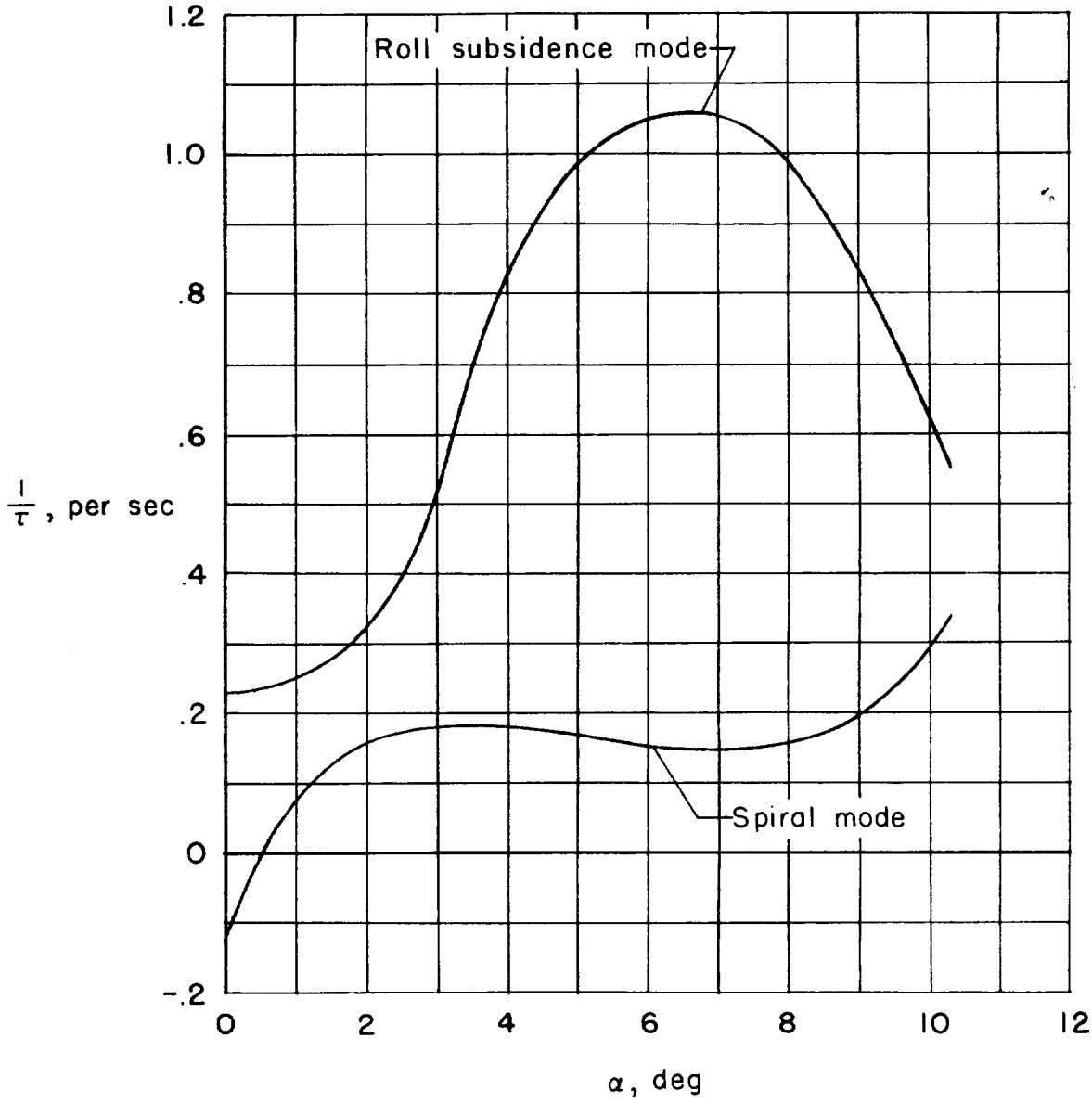

Figure 21.- Roll subsidence and spiral time constants for the simulated airplane; V = 300 feet per second, center of gravity at $0.51\bar{c}$.

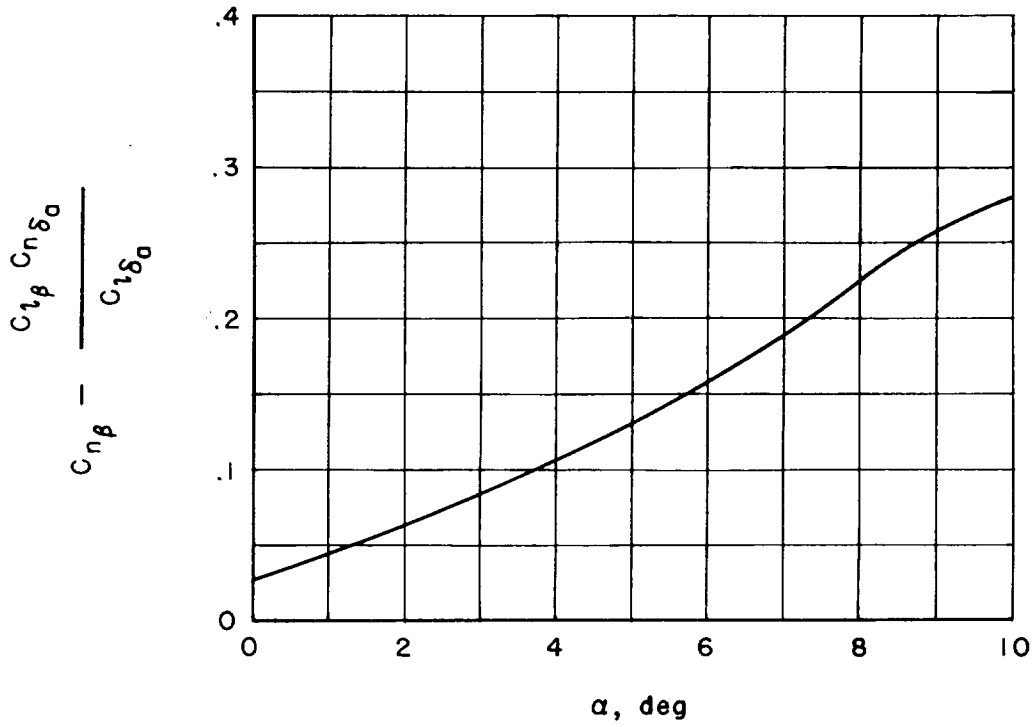

Figure 22.- Variation of roll divergence parameter with α for simulated airplane; center of gravity at $0.51\bar{c}$.

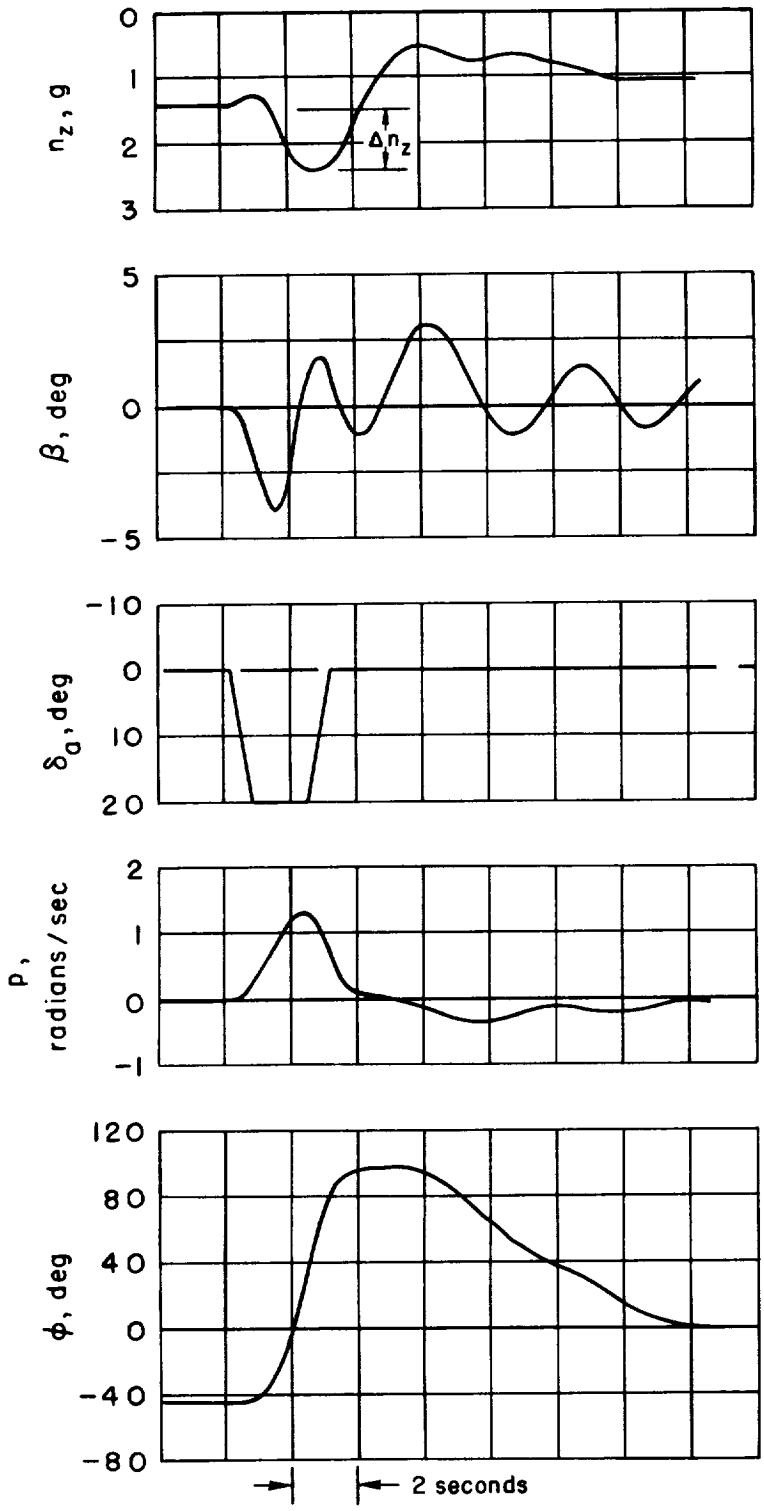

Figure 23.- Aileron roll of the simulated airplane from $\varphi = -45^\circ$ to $\varphi = 45^\circ$; V = 300 feet per second, center of gravity at $0.51\bar{c}$.

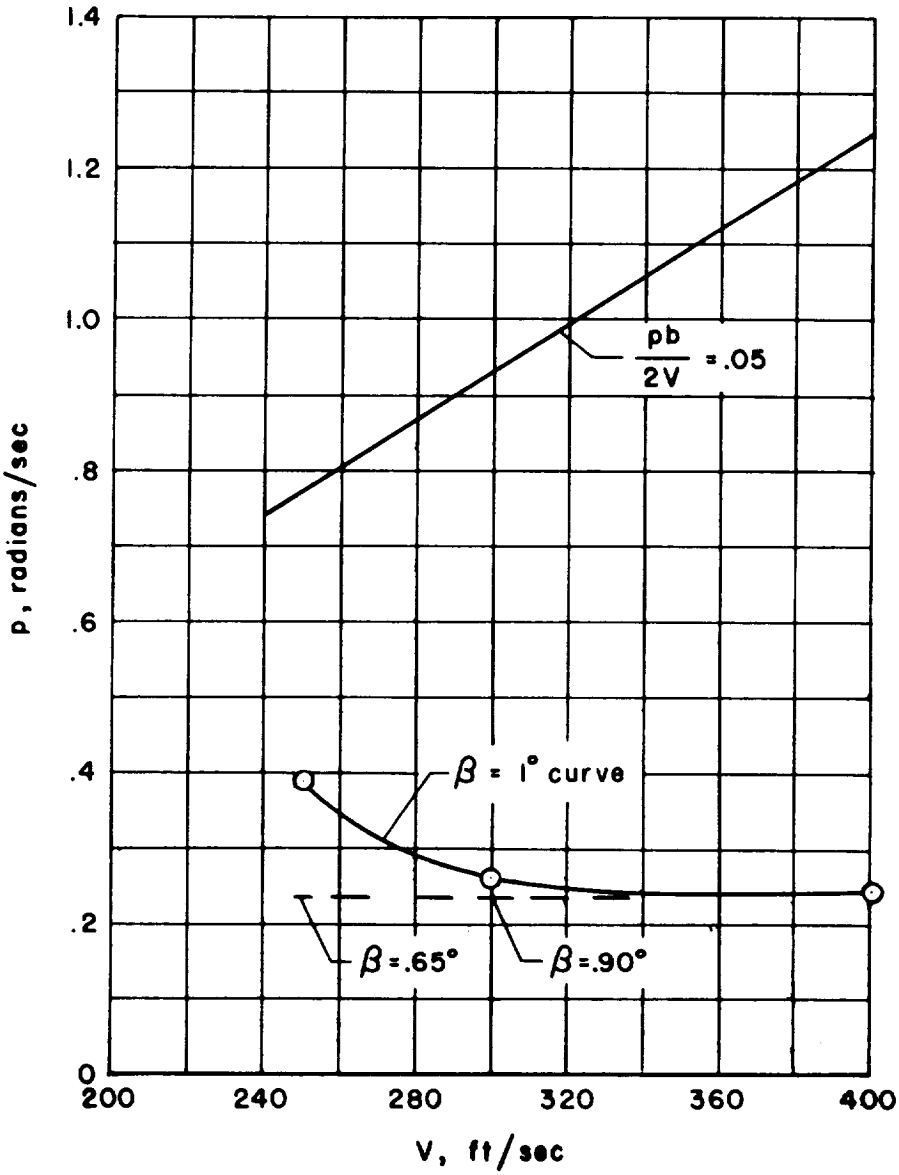

(a) Maximum roll rates obtainable with less than 1° sideslip.

Figure 24.- Aileron rolls of the simulated airplane from $\varphi = -45^\circ$ to $\varphi = 45^\circ$; center of gravity at $0.51\bar{c}$.

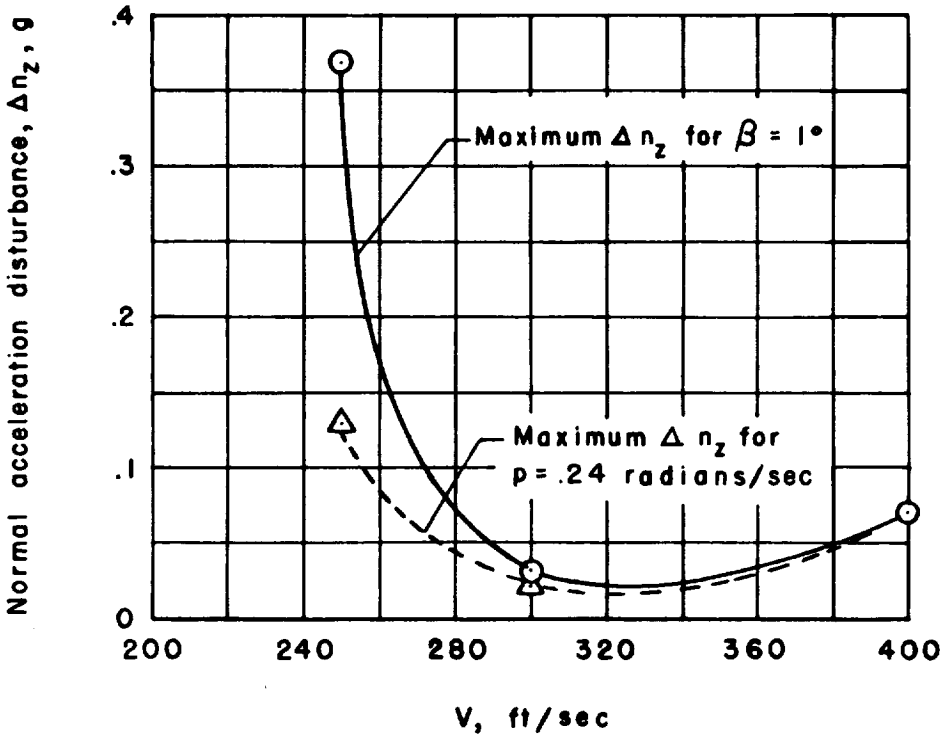

(b) Normal acceleration coupling.

Figure 24.- Concluded.

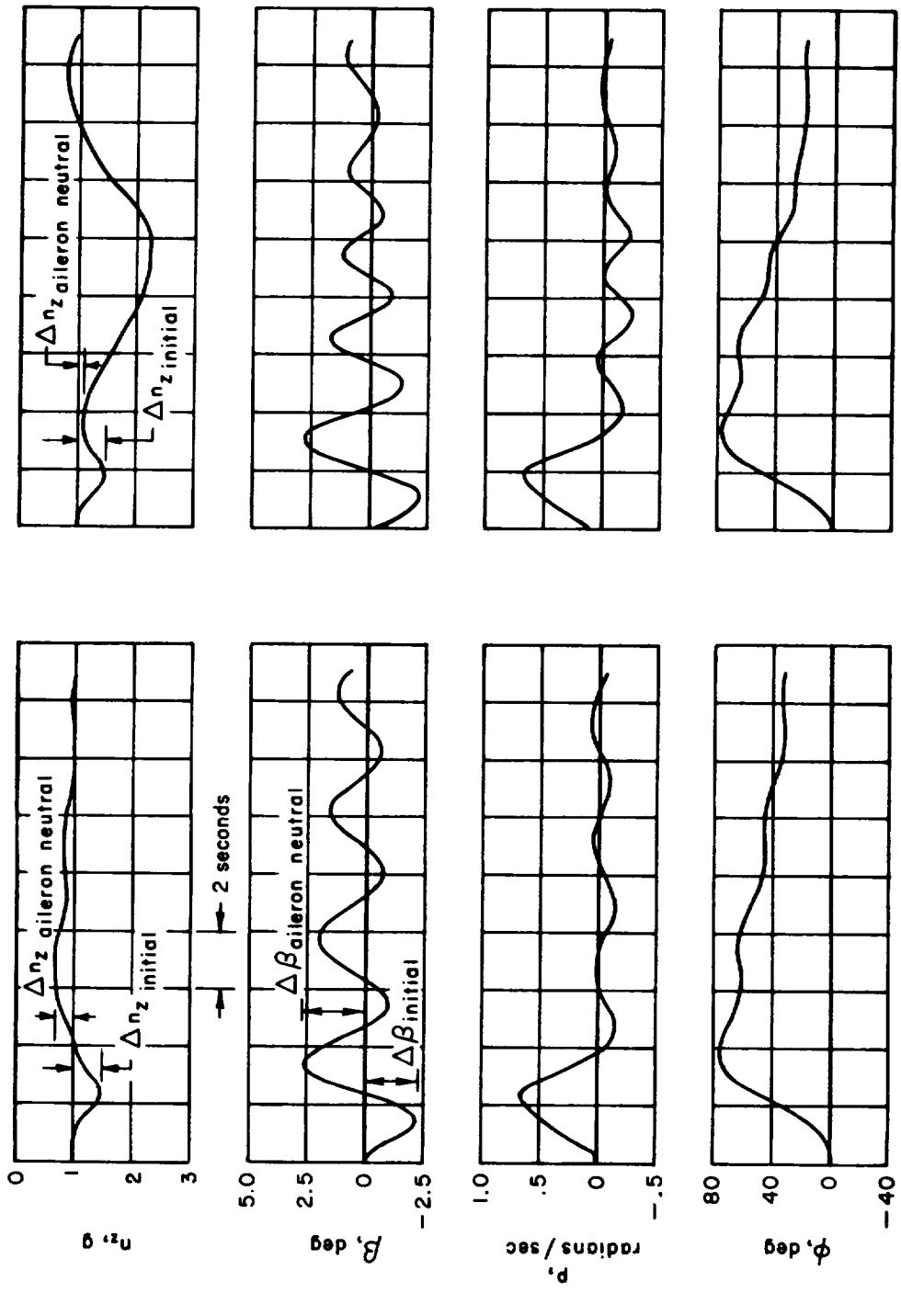

(a) No attempt to coordinate turn.

(b) n_z coordinated with φ to prevent loss of altitude.

Figure 25.- Aileron rolls of the simulated airplane from $\varphi = 0^\circ$ to $\varphi = 45^\circ$; V = 300 feet per second, center of gravity at 0.51c̄.

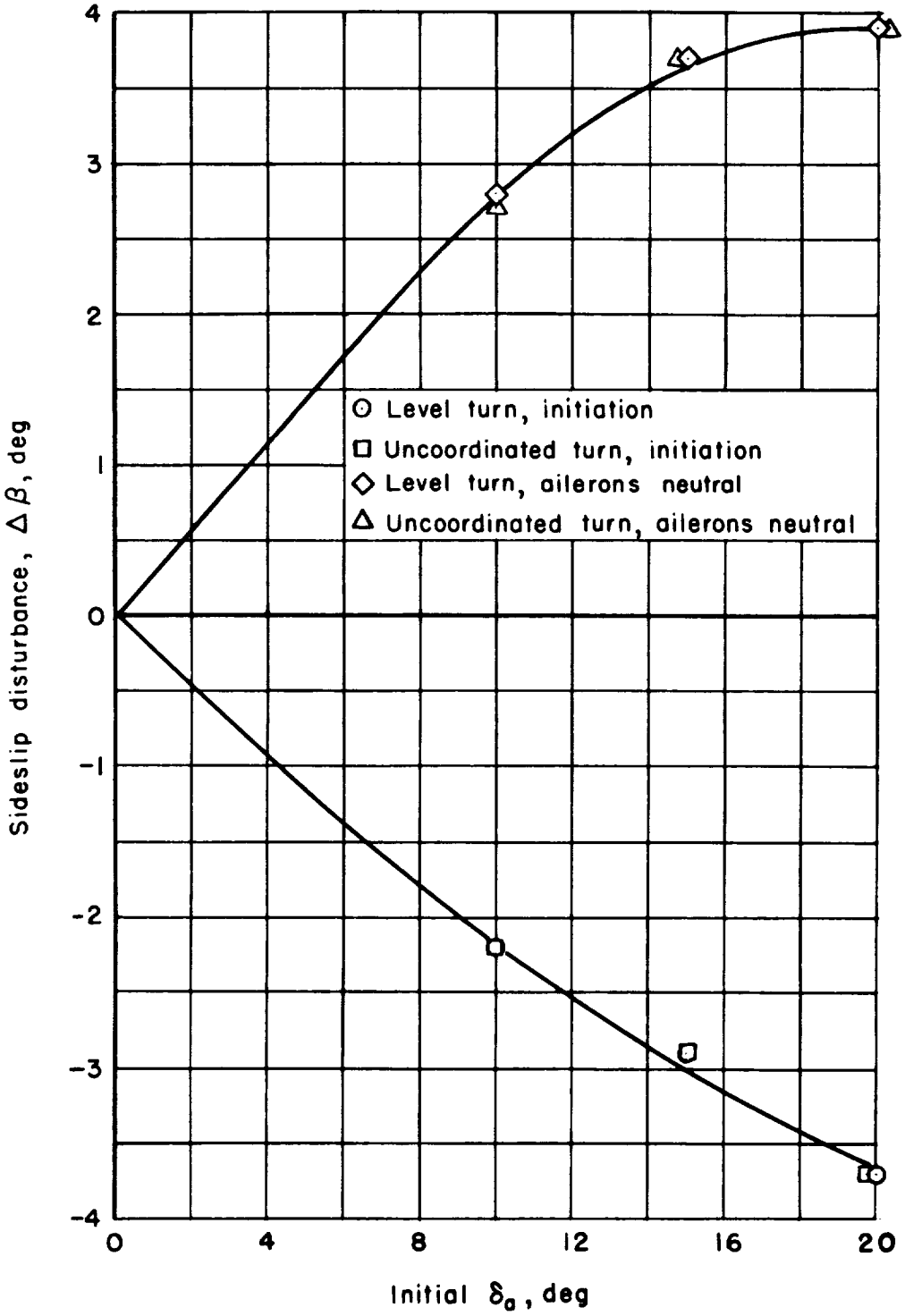

(a) Induced sideslip.

Figure 26.- Turns of the simulated airplane from trimmed level flight to $\varphi = 45^{\circ}$; V = 300 feet per second; center of gravity at $0.51\bar{c}$.

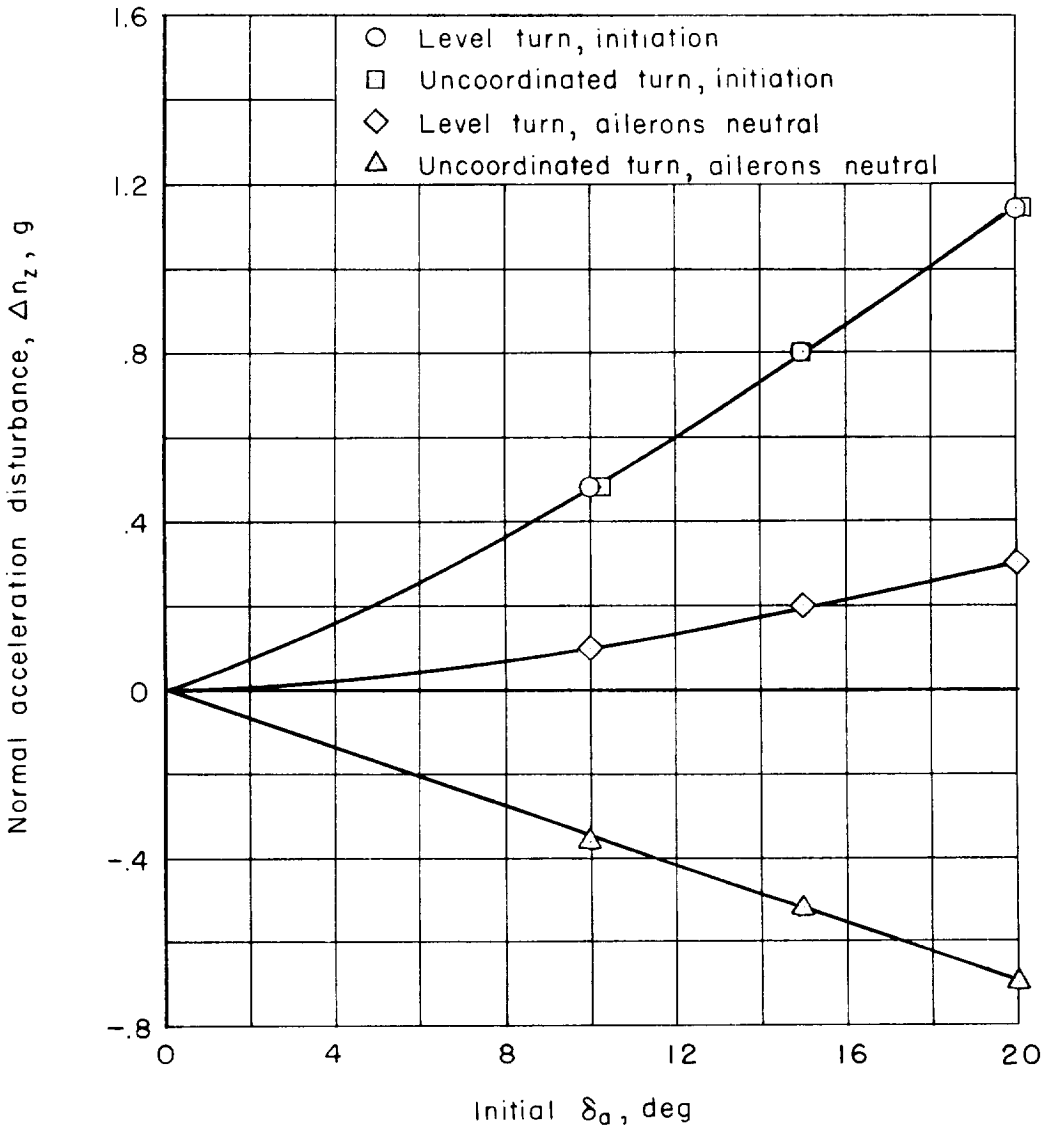

(b) Induced normal acceleration.

Figure 26.- Concluded.

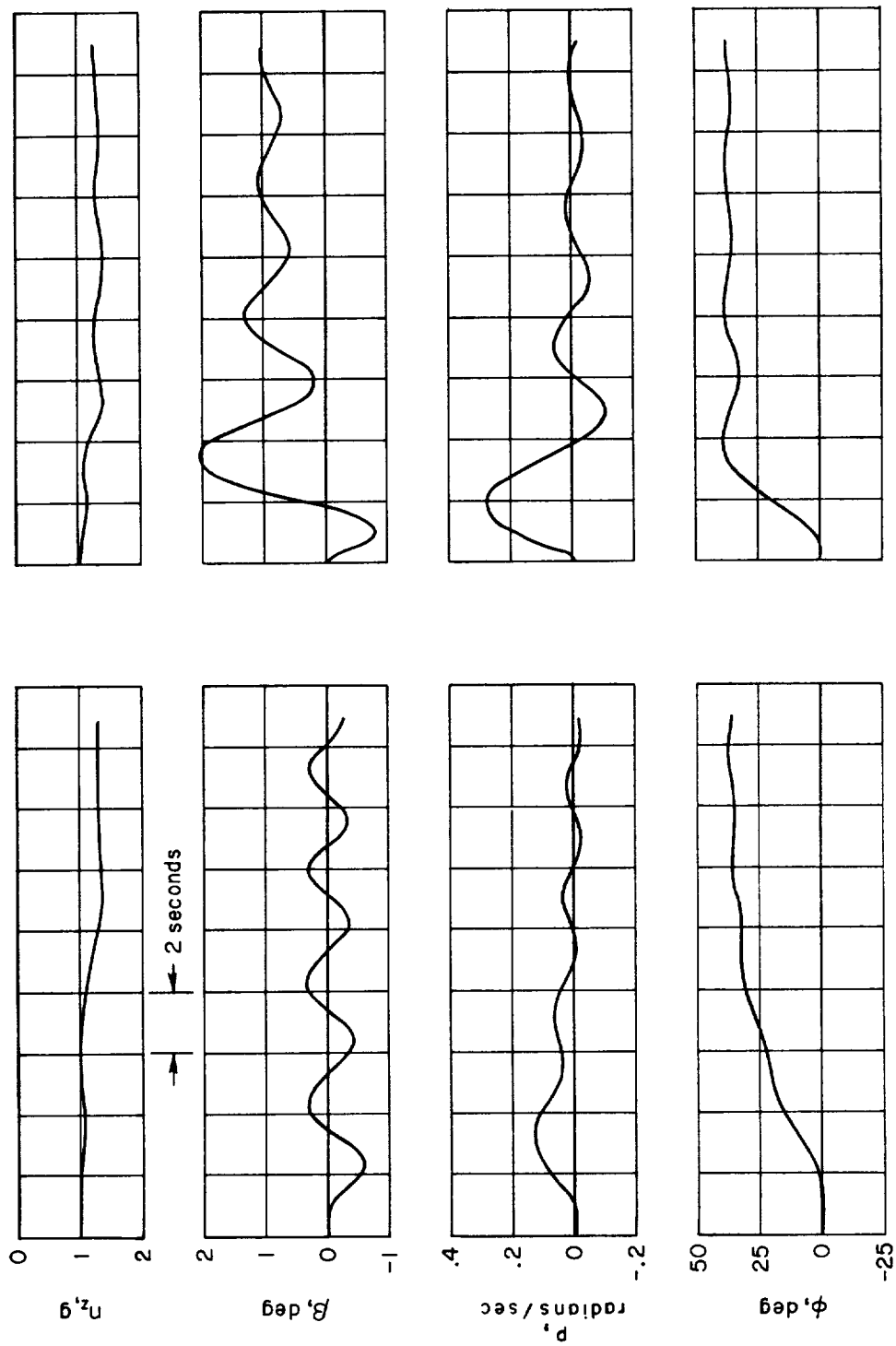

(a) No damper.

(b) With yaw damper.

Figure 27.- Two-control 1.3g turn of the simulated airplane with and without yaw damper; V = 300 feet per second, center of gravity at 0.51$\bar{c}$.

NASA MEMO 3-5-59A
National Aeronautics and Space Administration.
STABILITY AND CONTROL CHARACTERISTICS AT SUBSONIC SPEEDS OF A FLAT-TOP ARROWHEAD WING-BODY COMBINATION. Donald A. Buell and Norman S. Johnson. March 1959. 54p. OTS price, $1.50. (NASA MEMORANDUM 3-5-59A)

The configuration tested at Mach numbers of 0.22 to 0.90 had a wing with sweepback of 78.9° and a cathedral of 45° on the outer panels. Static- and dynamic-stability coefficients and control-surface effectiveness, including ground effects, were determined and the aerodynamic derivatives and criteria of stability and control were computed. An analog computer study was made in five degrees of freedom and the maneuvering characteristics of the airplane were determined.

I. Buell, Donald A.
II. Johnson, Norman S.
III. NASA MEMO 3-5-59A

NASA

NASA MEMO 3-5-59A
National Aeronautics and Space Administration.
STABILITY AND CONTROL CHARACTERISTICS AT SUBSONIC SPEEDS OF A FLAT-TOP ARROWHEAD WING-BODY COMBINATION. Donald A. Buell and Norman S. Johnson. March 1959. 54p. OTS price, $1.50. (NASA MEMORANDUM 3-5-59A)

The configuration tested at Mach numbers of 0.22 to 0.90 had a wing with sweepback of 78.9° and a cathedral of 45° on the outer panels. Static- and dynamic-stability coefficients and control-surface effectiveness, including ground effects, were determined and the aerodynamic derivatives and criteria of stability and control were computed. An analog computer study was made in five degrees of freedom and the maneuvering characteristics of the airplane were determined.

I. Buell, Donald A.
II. Johnson, Norman S.
III. NASA MEMO 3-5-59A

NASA

NASA MEMO 3-5-59A
National Aeronautics and Space Administration.
STABILITY AND CONTROL CHARACTERISTICS AT SUBSONIC SPEEDS OF A FLAT-TOP ARROWHEAD WING-BODY COMBINATION. Donald A. Buell and Norman S. Johnson. March 1959. 54p. OTS price, $1.50. (NASA MEMORANDUM 3-5-59A)

The configuration tested at Mach numbers of 0.22 to 0.90 had a wing with sweepback of 78.9° and a cathedral of 45° on the outer panels. Static- and dynamic-stability coefficients and control-surface effectiveness, including ground effects, were determined and the aerodynamic derivatives and criteria of stability and control were computed. An analog computer study was made in five degrees of freedom and the maneuvering characteristics of the airplane were determined.

I. Buell, Donald A.
II. Johnson, Norman S.
III. NASA MEMO 3-5-59A

NASA

NASA MEMO 3-5-59A
National Aeronautics and Space Administration.
STABILITY AND CONTROL CHARACTERISTICS AT SUBSONIC SPEEDS OF A FLAT-TOP ARROWHEAD WING-BODY COMBINATION. Donald A. Buell and Norman S. Johnson. March 1959. 54p. OTS price, $1.50. (NASA MEMORANDUM 3-5-59A)

The configuration tested at Mach numbers of 0.22 to 0.90 had a wing with sweepback of 78.9° and a cathedral of 45° on the outer panels. Static- and dynamic-stability coefficients and control-surface effectiveness, including ground effects, were determined and the aerodynamic derivatives and criteria of stability and control were computed. An analog computer study was made in five degrees of freedom and the maneuvering characteristics of the airplane were determined.

I. Buell, Donald A.
II. Johnson, Norman S.
III. NASA MEMO 3-5-59A

NASA